A Large Area CCD Camera for the Schmidt Telescope at the Venezuelan National Astronomical Observatory

C. Baltay[1], J. A. Snyder[1,2], P. Andrews, W. Emmet, B. Schaefer[3], J. Sinnott[4]

Physics Department, Yale University, New Haven, CT, 06520–8121, USA

C. Bailyn, P. Coppi[5], A. Oemler[6], C. N. Sabbey[7], S. Sofia, W. van Altena, A. K. Vivas

Astronomy Department, Yale University, New Haven, CT, 06520–8101, USA

C. Abad, C. Briceño, G. Bruzual, G. Magris, J. Stock, F. Della Prugna, Ge. Sánchez, Gu. Sánchez, H. Schenner

Centro de Investigaciones de Astronomía, Mérida, Venezuela

B. Adams, M. Gebhard, R. K. Honeycutt, J. Musser

Indiana University, Bloomington, IN, 47405–7105, USA

F. Harris[8]

Universities Space Research Association, USNO, Flagstaff, AZ, 86002–1149, USA

and

J. Geary

Harvard-Smithsonian Center for Astrophysics, 60 Garden Street, Cambridge, MA 02138, USA

ABSTRACT

[1]Also Astronomy Department, Yale University, New Haven, CT, 06520–8101, USA

[2]Send correspondence to jeffrey.snyder@yale.edu

[3]Present location University of Texas, Austin, TX, 78712, USA

[4]Present location Cornell University, Ithica, NY, 14853-1501, USA

[5]Also Physics Department, Yale University, New Haven, CT, 06520–8121, USA

[6]Also Carnegie Observatories, Pasadena, CA, 91101, USA

[7]Present location: Bogle Investment Management, Wellesley, MA, 02481, USA

[8]Present location: U. S. Naval Observatory, Flagstaff, AZ, 86002–1149, USA

We have designed, constructed and put into operation a large area CCD camera that covers a large fraction of the image plane of the 1 meter Schmidt telescope at Llano del Hato in Venezuela. The camera consists of 16 CCD devices arranged in a 4×4 mosaic covering $2.3^\circ \times 3.5^\circ$ of sky. The CCDs are 2048×2048 LORAL devices with $15\,\mu$m pixels. The camera is optimized for drift scan photometry and objective prism spectroscopy. The design considerations, construction features and performance parameters are described in the following article.

Subject headings: instrumentation: detectors, surveys, cosmology

1. Introduction

Schmidt telescopes are the instrument of choice for surveys of large areas of the sky because of their large field, typically of the order of $4^\circ \times 4^\circ$. However, these telescopes have large, curved image planes and are difficult to instrument with silicon detectors. Until now, these telescopes have been used with photographic plates and no Schmidt telescope had its image plane fully instrumented with silicon CCD detectors. The Near–Earth Asteroid Tracking (NEAT) project has recently instrumented the Palomar 48" Oschin Schmidt telescope with three 4080×4080 CCDs (Pravdo 2002). This camera covers a total of ~ 3.75 square degrees of the ~ 36 square degree field of view. A project is underway to fully instrument this telescope.

We, the QUEST collaboration,[9] have designed, constructed and put into operation, a large area CCD camera that covers a large fraction of the image plane of the 1 meter Schmidt telescope at the Venezuelan National Astronomical Observatory located at Llano del Hato and operated by CIDA.[10] This is one of the five largest Schmidt telescopes in the world; its properties are summarized in table 1. A picture of the camera is shown in figure 1. The camera is located at the prime focus inside the telescope tube as shown in figure 2.

The scientific motivation for building this camera was to carry out a large area survey of a band of the sky centered on the celestial equator and about $\pm 6^\circ$ wide in declination. The initial plan was to divide the observations between objective prism spectroscopy, imaging with four essentially simultaneous color filters, and repeated scans of a 250 square degree area of the sky for variability studies. Some of the scientific results expected from such a survey were a quasar survey based on quasar selection with three different techniques: selection by the presence of broad emission lines

[9]QUEST is short for the Quasar Equatorial Survey Team, and is a collaboration between groups from Yale University, Indiana University, Centro de Investigaciones de Astronomía (CIDA), and Universidad de Los Andes (Mérida, Venezuela).

[10]Research reported herein is based on data obtained with the 1m Schmidt telescope at the Venezuelan National Astronomical Observatory, Mérida, Venezuela, operated by the Centro de Investigaciones de Astronomía (CIDA) and funded by the Ministerio de Ciencia y Technología and the Fondo Nacional de Ciencia y Technología of Venezuela.

using the objective prism, color selection with UBV and BVR colors, and variability selection. The variability survey was included to search for type Ia supernovae, gamma ray bursters, new solar system objects (like asteroids and Kuyper belt objects), and RR Lyrae stars.

The large area CCD camera consists of 16 CCD devices arranged in a 4×4 mosaic (see fig. 3) covering $2.3^\circ \times 3.5^\circ$ of sky. The individual CCDs are 2048×2048 LORAL devices with $15\,\mu$m pixels. There are gaps between the CCDs in the East–West direction so that the effective area covered is 5.4 square degrees. The properties of the camera are summarized in table 2. The camera has been designed to operate in drift scan mode,[11] which is also referred to as time–delay integration (TDI) mode (McGraw et al. 1986). In this mode the telescope is locked into a fixed position at a given declination angle. The CCD array is oriented with the columns of pixels in the clocking direction lined up precisely in the East–West direction, and the CCDs are clocked synchronously with the motion of the star images across each CCD. Each star image thus crosses four CCDs, one in each row of CCDs. Each row of CCDs can have a filter of a different color in front of it so the camera can collect images in each of four colors essentially simultaneously. The camera thus has a 100% duty cycle (i.e., data is collected continuously) and no time is lost due to readout time or telescope slewing time. Since the telescope is locked into fixed position and is not tracking, the system is very stable and produces more accurate photometric measurements. Photometric precision is further enhanced because each point in the sky is imaged by averaging over an entire column of pixels and thus pixel–to–pixel variations in sensitivity are minimized.

During a clear night, a 2.3° wide by 120° long strip, or approximately 250 square degrees, can be covered in each of four colors. The telescope is equipped with an objective prism covering the full aperture of the telescope and can be installed or removed on a daily basis. Thus, one can collect objective prism spectra over 250 square degrees of sky on a clear night. The camera was built at Yale University and Indiana University. It was installed at the prime focus of the telescope in 1997 and has been taking data routinely since November 1998.

In the following sections, we will describe the principles of operation of the camera (§2), give a detailed description of the camera (§3), the detector control system and electronics (§4), the data analysis software (§5), and the performance of the apparatus to date (§6).

2. Principles of Operation of the Camera

If the camera were used to drift scan along the equator, the images of stars would follow straight lines and move at the same rate across the image plane. However, at declinations other than the equator, the stars will follow arcs of circles and stars at different North-South positions will move at different rates. In drift scanning, the sagittas due to the first effect will smear the images in the North-South direction, and due to the second effect some of the stars will not be

[11] We thank Steve Shectman for many interesting discussions concerning the technique of drift scanning.

exactly synchronous with the CCD clocking rates and thus will be smeared in the East-West direction. In order to keep these effects at an acceptable level, i.e. to keep the smearing of the point spread function below about one arc second in any direction, we rotate each CCD by an amount dependent on the declination being scanned in such a way that the clocking direction of each CCD is tangential to the arcs that the stars are moving in at that location in the array. This is accomplished by mounting each of the four CCDs in a North-South row on an Invar[12] bar, which we call a "finger." Each of the four fingers can be rotated by a different amount by cams which are driven by external, computer controlled stepper motors. An exaggerated sketch of this scheme is shown in figure 4. For convenience, we label the fingers 1, 2, 3, and 4, and the columns of CCDs A, B, C, and D, as shown in figure 3. This figure also shows the pivot points and the cams used to rotate the fingers. In addition, each column of CCDs is scanned along a slightly different declination, and therefore, the parallel clocks reading out the CCDs are synchronized at slightly different rates.

The radius r_δ of the star tracks (i.e. the arcs of circles along which the image of a star moves in drift scanning) on the image plane of a telescope with focal length f at a declination δ is to a good approximation given by:

$$r_\delta = \frac{f}{\tan\delta}.$$

The parallel clock rate ν_δ for reading out a CCD in such a way that the motion of the charge is synchronous with the motion of the star image across the CCD at a declination δ is given by:

$$\nu_\delta = \frac{\Omega f}{a}\cos\delta.$$

where $\Omega = 72.7\mu$radians/sec is the rotation rate of the Earth, f is the focal length of the telescope, and a is the pixel size on the CCD. For the Venezuelan Schmidt telescope and our pixel size, this gives:

$$\nu_\delta = 14.7\cos\delta \qquad \text{lines/second.}$$

In drift scanning along the equator, the readout parallel clocks are thus synchronized at approximately 14.7 lines/second. At this rate, a star image takes 140 seconds to cross a CCD. This gives an integration or exposure time of 140 seconds. At higher declinations, the clocking rate is somewhat slower giving a slightly longer exposure time. In drift scan mode, this exposure time is governed by the rotation of the earth and can not be changed. However, since each star crosses four CCDs, these can be added for an effective exposure time of 560 seconds. In cases where even longer exposure times are desirable, repeated scans of the same area of sky can be performed and co–added.

The angle by which the CCD support fingers (see figure 4) have to be rotated to keep the

[12]Invar is a stainless steel alloy that has a relatively low coefficient of thermal expansion.

clocking direction of the CCDs tangent to the star tracks on the image plane at a declination δ is:

$$\Delta\theta = \frac{d}{f}\tan\delta$$

where d is the distance of the pivot point of each finger from the camera centerline ($d = \pm 7.5$ cm for fingers 1 and 4 and ± 2.5 cm for fingers 2 and 3). Thus, for example, the top finger (1) has to be rotated about 0.15° for $\delta = 6°$, which is very small but nevertheless quite important to keep the image sizes small. As mentioned above, the four columns of CCDs scan along slightly different declinations and thus have to be clocked at slightly different rates. For example, with the camera scan centered at $\delta = 6°$, the four columns have to be clocked at 14.638, 14.626, 14.613, and 14.598 lines/second, respectively. Again this variation is very small but nevertheless quite important. The detailed implementation of this scheme is to clock all four columns at the same rate but drop clock pulses at different rates in the four columns to produce the average clock rates required. The fast serial readout clock is 50 kHz for all of the CCDs in the array.

The scheme described above for varying the rotation and clock rate synchronization of the different CCDs in the array removes the dominant effects that smear the images. There are, however, residual effects due to the sagitta of the image motion and spread in the rate of motion of the images across the finite width of a single CCD, as illustrated in figure 5. For a CCD with length l (in the E-W direction) and width w (in the N-S direction), the residual smearing of the image size Δx and Δy, in the E-W and N-S directions respectively, scanning at a declination δ, is given by:

$$\Delta x = \frac{1}{8}\frac{l^2}{f}\tan\delta$$

$$\Delta y = \frac{1}{2}\frac{lw}{f}\tan\delta$$

where f is the focal length of the telescope. This residual smearing limits the range of declinations at which this camera can be used in the drift scanning mode without intolerable degradation of the image sizes.

The design has been optimized in such a way that the residual image smearing is kept below 1 arcsec for declinations up to ±6°. Given the typical seeing at the Llano del Hato site, we can drift scan at declinations up to ±12° with no appreciable degradation of image quality. This is sufficient for the equatorial survey for which the camera has been designed. Of course, the camera can be operated in a conventional point and stare mode to cover regions of the sky above these declinations.

Another complication of the design was due to the fact that the image plane of a Schmidt telescope is not flat but has the shape of a convex spherical surface. To arrange the CCDs in such a shape would have been cumbersome. Instead, we designed, and had built, a 30 cm diameter field flattener lens that covered the entire image plane. This lens produced a flat image plane and, in addition, corrected for the pincushion distortion inherent in the telescope to a level where the degradation of the image shapes were negligible.

The depth of field of the Venezuelan Schmidt telescope is quite shallow. For this reason, the front surfaces of the 16 CCDs, including the motion of the finger mounts, had to be kept in a plane to a tolerance of less than $\pm 25\,\mu$m. It required great care in the precision machining and the alignment procedures to achieve this precision.

During the commissioning period, after the camera had been installed in the telescope, a great deal of effort was expended to align the plane of the CCDs with the focal plane of the telescope. Once this had been achieved, however, it was quite stable and required no further adjustment. Typically, before each nights' data taking the focus of the telescope, the rotational position of the fingers, and the synchronized read out rate, which have been set by the control computers for the appropriate declination, were checked by looking at the shape and size of stellar images.

There is an objective prism designed for the Venezuelan Schmidt telescope which covers the entire 1m aperture. By aligning the dispersion direction of the prism along the drift direction, we can obtain spectra over the entire survey area. The prism is made of UBK7 for good ultra-violet transmission down to the atmospheric cutoff. With a prism angle of 3.3°, the dispersion is 650 Å/mm at 4350 Å. In combination with the QUEST camera, this corresponds to a spectral resolution of 10 Å per pixel at this wavelength which is more than sufficient to detect quasars.

3. Description of the QUEST Camera

The CCD camera is located at the prime focus of the Venezuelan Schmidt, inside the telescope about 3 m from the 1.5 m primary mirror, with the CCDs facing the mirror (see figure 2). The outside dimensions of the camera have to be as small as possible to fit mechanically at the prime focus and to obscure as small a part of the incoming beam as possible. The outside of the camera has to be kept at ambient temperature so as not to induce any turbulence in the air inside the telescope.

3.1. The CCDs

The heart of the camera is a mosaic of 16 CCDs arranged as shown in figure 3. Each CCD consists of 2048×2048 pixels, each $15\,\mu\text{m} \times 15\,\mu$m, as shown in figure 6. The CCDs were designed by John Geary of the Harvard–Smithsonian Center for Astrophysics (CfA) and were part of a multi–lot fabrication run by LORAL (20 four inch diameter wafers per lot with four CCDs per wafer). These fabrication lots were initially purchased by various U.S. and European observatories and we were able to obtain a few individual unused devices from a number of these observatories.[13] Most of the devices were three–side buttable with 21 readout pads along a single edge; a few of

[13]We are grateful to John Geary (CfA), Edgar Smith (EST), Jerry Lupino (Hawaii), Kent Cook (Los Alamos) and Fabio Bartoletto (Padua) for these devices.

them were two–side buttable. The two–side buttable CCDs could be used on the outside columns (A and D) with no interference. Each of these devices had a number of bad pixels and some bad columns but this does not significantly affect their performance.

These devices are unthinned (500 μm thick) and are used in the front illluminated mode. As such, the quantum efficiency drops to zero below 4000 Å. Since we need sensitivity in the ultraviolet we applied a 2.5 μm thick layer of a wavelength shifting compound to the front surface of each device. This compound absorbs light in the UV and reemits it in the visible. We have not carried out detailed quantum efficiency measurements but we believe that the QE is similar to the typical response of front illuminated LORAL CCDs, as shown in figure 7 (**?**, Adapted from)]loral, with the modification at short wavelength due to the wavelength shifting compound. The properties of the CCDs are summarized in table 3.

The read noise of the CCDs, including the noise from the electronics and pickup in the cabling, etc., is around 10 electrons, but with some spread. The best we have seen is 7 electrons noise, and some of the devices in the camera are as poor as 20 electrons noise. The measurement of the dark current versus temperature on a typical CCD is shown in figure 8. The dark current extrapolates to $\sim$ 250 pA/cm^2 at 20°C, and falls a factor of 2 with with each 5°C temperature drop. The CCDs in the camera are typically operated at -70°C. The response of the CCDs is linear to a good approximation up to the full well capacity, which varies from 30,000 to over 60,000 electrons.

3.2. The Field Flattener Lens

The Venezuelan Schmidt normally has a focal plane that has the shape of a convex spherical surface. To allow the CCD array to be in a flat plane we have designed a field flattener lens to reimage the focal plane. Great care had to be exercised in this design to keep pincushion and other distortions below a few microns in the image plane to allow the camera to be used in a drift scan mode. The lens was designed by the QUEST collaboration and was manufactured by Coastal Optical Systems of Riviera Beach, Florida. The lens has a 30 cm diameter and is also used as the vacuum window at the front of the detector. The lens is biconvex, with two spherical surfaces of radius of curvature of 2595 mm and -1725 mm respectively. It is 25 mm thick in the center and 14 mm thick at the edges. Careful finite element stress analysis calculations have been carried out to show that the lens is strong enough to serve as a vacuum window and the deflection is small enough not to distort the optical properties of the lens unduly. The lens is made of fused silica, Corning 7940, which has good transmission in the ultraviolet as well as over the whole required wavelength range. The lens does not have an antireflection coating. The lens is located about 2 cm in front of the CCD image plane. We have examined the image sizes and shapes at different locations on the image plane. No variation or degradation as a function of distance from the center of the image plane has been observed (see figure 9). We therefore believe that this lens has flattened the field to an acceptable level.

3.3. The Camera Dewar

To be able to cool the CCDs to $-70°$C they have to be in a vacuum enclosure. The detector housing is thus a vacuum vessel cylindrical in shape 16 inches in diameter, about 5 inches deep as shown in figure 10. The front face has a 12 inch diameter circular vacuum window made of fused silica for good UV transmission. This window also serves as the field flattener lens discussed above. The back plate of the housing has the mounting bracket on it to attach the detector to the telescope. The back plate also has penetrations for the vacuum pump port, the vacuum gauge, refrigerant liquid in and out, and all of the electrical feedthroughs. The housing is made of aluminum, polished on the inside to reduce radiative heat loss, and anodized flat black on the outside to reduce reflections and glare.

3.4. Refrigeration

The conventional method of cooling the CCDs in astronomical cameras is to have a liquid nitrogen dewar inside the camera vacuum enclosure. In our case, this would have been a feasible solution but would have made the detector quite bulky because of the large volume of liquid needed to cool the large CCD array, and would present a logistic problem since at this time there is no liquid nitrogen available at the observatory. We have found a much simpler and maintenance free solution, namely a closed loop refrigerator using a liquid freon coolant that can operate in the -60 to $-80°$C temperature range. Such a refrigerator was commercially available, a model RC210C0 from FTS Systems in Stone Ridge, New York. The refrigeration unit is located near the North pier of the Schmidt telescope, and a vacuum jacketed cryogenic liquid transfer line with the appropriate flexible joints was installed to carry the coolant to and from the detector inside the telescope. Inside the detector the coolant circulates through cooling loops attached directly to the invar support bars to which the CCDs are attached, insuring a temperature of all of the CCDs uniform to $\sim 1°$C.

The overall temperature can be regulated by controlling both the temperature and the circulation rate of the coolant. The camera's overall heat load is ~ 30 watts, dominated by the heat radiated in through the large vacuum window. There are heaters attached to the body of the camera to maintain the outside of the camera at ambient temperature.

3.5. The Vacuum System

The camera dewar is operated at a vacuum of $\sim 10^{-4}$ torr, which is sufficient to keep the convective heat loss at a negligible level. The vessel is evacuated by a turbomolecular pump preceeded by a roughing pump. These pumps are not connected during observations. In fact, once the vessel is evacuated, the vacuum usually lasts for weeks so the pumps are connected only periodically.

3.6. The CCD Support Structure

The individual CCDs were packaged at Yale. The CCDs were epoxied to a ~ 3 mm thick invar plate approximately 3.1 cm $\times$ 3.1 cm large. A small circuit board was epoxied next to the invar plate and the electrical connections from the CCD to this circuit board were achieved by wire bonding to this board (see fig. 11). The CCD packages are mounted on four invar bars (fingers) each 0.25 inches thick, 1.0 inches wide and 11 inches long. These four fingers in turn are attached to a 14 inch diameter invar support plate 0.5 inches thick (see fig. 3). This plate has a large rectangular opening in the center to allow the electrical connections from the CCDs to pass through to the preamplifier board located at the back of the dewar under this plate. The Schmidt telescope has a very shallow depth of field ($\pm 25\,\mu$m). Therefore, all of the CCDs have to be located in the focal plane to a precision smaller than this. All of the invar bars and the support plate were ground to $5\,\mu$m precision and all joints are spring loaded to ensure the required precision. The invar parts were coated with an Armoloy[14] coating to prevent corrosion. After the entire system was assembled, a detailed optical survey showed that the front surfaces of all of the CCDs were in a plane with an rms scatter of $11\,\mu$m.

The invar fingers pivot at one end and their rotational position is controlled by cams located near the other end under the invar support plate. The shafts of the four cams penetrate the back plate of the dewar to the gears and stepping motors located outside of the dewar. The invar support plate is supported from the dewar back plate by three standoffs which are 10 cm long hollow stainless steel tubes to reduce the heat conduction to an acceptable level.

3.7. Color Filters

The filter box is located a few centimeters in front of the vacuum window/field flattener lens. Filter trays can be easily inserted or removed manually. A filter tray consists of four filters of different colors, each filter being 5.0 cm wide and 25.0 cm long. Each individual filter is located in front of one row of CCDs so that in the course of a drift scan star images pass through each of the four filters in turn so that data can be collected in four colors essentially simultaneously. A sketch of a filter tray is show in figure 12. Several filter trays exist and the individual filters can be shuffled to make up filter trays in any desired combination. The available filter colors and their wavelength bands are listed in table 4. These filters were designed specifically for the QUEST camera but they resemble the Johnson color system (Bessel 1990) quite closely. The optical thickness of the different filters were designed such that the entire system is parfocal.

There is a grid of five nichrome wires located in the filter box with the wires running along the edges of the individual filters. During conditions of high atmospheric humidity a current is passed

[14] Armoloy is a thin, dense chromium coating that is low friction, corrosion resistant and very hard.

through these heater wires to eliminate the condensation on the vacuum windows and the filters. This system has turned out to be quite effective.

3.8. The Shutter Box

The camera shutter is located in front of the filter box. The requirements on this shutter are to have a 12 inch diameter clear opening but that no part of the shutter box extend beyond the 16 inch diameter of the camera since the camera was located at the prime focus of the telescope and obscuration of the light path was to be minimized. No such shutter was commercially available so a shutter was custom designed and built for this purpose. It is an iris type shutter with 22 thin stainless steel shutter blades. The shutter is computer controlled and can open or close in about half a second.

4. Detector Control System and Readout Electronics

The electronics used to read out the camera are based on the CCD controller developed for the U. S. Naval Observatory and the Observatories of the Carnegie Institute of Washington by FHH Harris Engineering. A block diagram of the readout electronics is shown in figure 13. The heart of the system is a two board set, consisting of a digital board and an analog board, responsible for the clocking and readout of a single CCD. The phase clocks are generated on the digital board as outputs of a state machine which is implemented using field programmable logic devices (PLDs), allowing considerable flexibility in the clock waveforms. The analog board amplifies and digitizes the CCD video output and provides the digitized video to the data acquisition system, and is capable of operation at a maximum readout rate of 100 kHz. In addition to this two board set for each CCD, the complete readout system includes a line clock generator and an interface card to the data acquisition computer. As the system is implemented for this camera, the interface card services four CCDs. Control of the detector operating mode is accomplished through a serial interface between the interface card and the digital boards. This mode control allows the selective readout of an individual CCD, selection of drift scan or snapshot mode, and reset and calibration of the control system.

The system interconnections are shown in figure 13. Each CCD video signal is provided to an analog board through a coax cable. All phase clocks and DC voltages required by the CCDs are generated on the digital board, and provided to the camera via shielded cable. There are three groups of interconnections between the controller electronics and the data acquisition system. The digitized video output is provided to the interface board via coax cable. The mode control is a slow serial interface between the interface card and the digital boards, as described above. Finally, each column of CCDs receives a separate line start signal, which is generated by a counter/timer card in the data acquisition computer. Each of these will be described in more detail below.

4.1. Analog Board

The analog board provides the amplification, processing, and conversion to digital values of the output of the CCD detector. The analog board communicates with the associated digital board through a backplane, located at the back of a rack in which the analog and digital boards are mounted. The input to the ADC section consists of a double–correlated sample and hold, which is implemented as a switched–input dual slope integrator. The rather complicated sample and hold circuit is required to eliminate sensitivity to variations in the pre–charge levels on the CCD output node. Prior to the delivery of a charge packet on the CCD to the charge sense node, that node is precharged to a positive potential. After the precharging of the sense node capacitance on the CCD via the reset clock applied from the digital board, the value of the voltage potential of the sense node has some uncertainty compared to previous precharge values. This uncertainty is due to the non–zero on–resistance of the reset switch and the Johnson noise associated with that resistance. The magnitude of this voltage uncertainty can be of order 300 electrons, and must be corrected for. The ADC digitizes the output of the sample and hold to 16 bits. The conversion rate of the ADC is 50 kHz.

4.2. Digital Board

The digital board provides the time-varying signals needed to operate the CCD detector and its associated analog processing electronics on the analog board. As mentioned earlier, the phase clocks are generated as outputs of a state machine having a total of 64 states, with state transitions occurring at a rate of 4 Mhz. The phase clocks are output from clock drivers, which take as inputs the logic–level outputs of the state machine, combining these with the DC voltage outputs of a set of bias generators, and applying a simple RC low pass filter, to produce the shaped, level–shifted signals required by the CCD.

4.3. Line Start Generator

The camera is intended to be operated in drift scan mode. In this mode of operation, each column of CCDs, corresponding to CCDs at a common declination, require a common line start clock, while different columns will require slightly different line start rates, dictated by the declination bands being viewed. The method by which this is implemented is to operate all columns at a common nominal line start rate, but to drop line start cycles for each column at a rate which gives the correct average line start rate for that column. This allows synchronous operation of the system, avoiding having large clock transisitons ($\sim$ 10 V) during the sensitive ($\sim$ 1 mV) charge readout time.

The line start generation circuitry consists of two components. The first is a commercial

timer/counter board (NI PCI-TIO-10) running in the primary data acquisition computer. This board generates the correct nominal line start rate, and, for each column, a cycle reject clock, which clocks at the rate at which lines starts are skipped on that column. Once programmed, this board functions without intervention from the data acquisition system. The second module in the line start circuitry is the line start generator. This board accepts the raw clocks produced by the timer/counter board, and generates the line starts used by the controller boards. These line starts are delayed by a fixed time interval to allow the data acquisition computer time to prepare for the line readout. The line start generator also provides a set of prompt interrupt lines to the data acquisition computer to notify the data acquisition system of an incoming line.

4.4. Data Acquisition Interface Card

A 4–channel PC interface to the controller system has been developed jointly at Princeton University and the U. S. Naval Observatory for the Sloan Digital Sky Survey (SDSS) project.[15] This card provides a DMA interface to four CCD inputs, as well as a serial output to the controller electronics which allows control of the camera operational mode.

4.5. Data Acquisition Computers

The data acquisition system is built around standard IBM PC compatible hardware. For a full description see Sabbey et al. (1998). Each column in the array (consisting of four CCDs), is controlled by one Pentium–based CPU. One controller board controls all 4 CCDs, sending commands and receiving data. Because all chips in the column (indeed, all in the detector) are clocked at the same rate, the entire data acquisition can be run as one synchronous process. This eliminates many timing headaches. The data is stored during the night on disks, and written to DLT tapes at the end of a night's observing. The four data acquisition computers run on the QNX operating system and are linked through two data storage computers to one central controlling computer via Ethernet. The control computer, running Linux as its operating system, organizes the data taking process, and monitors the quality of data during the night, using samples sent from the data taking machines over the ethernet connection. A block diagram of the data acquisition hardware is shown in Figure 14.

[15]We are grateful to Jim Gunn (Princeton University) for supplying the PC interface boards.

5. Data Rates and Data Analysis Software

5.1. Data Rates

As discussed in §4.1 above, the analog to digital converter (ADC) outputs 16 bits for the signal from each pixel. The calibration of the electronics varies slightly from channel to channel but is in the vicinity of 1 electron per ADU (analog to digital conversion unit). In the drift scan mode the entire 64×10^6 pixels of the array are read out once every 140 seconds with 2 bytes per pixel, resulting in a data rate of approximately 1 megabyte per second. This data is stored on disks and written on a DLT tape in the morning after the observation night. A clear 8 hour night produces about 28 gigabytes of data. With appropriate compression (Sabbey 1999a) this will fit on a single DLT IIIXT tape. These tapes are the raw data input for the offline processing.

The software to process such a large volume of data is not trivial. The QUEST collaboration has developed three different software pipelines to analyze this data: a) the photometric pipeline to analyze data taken with the multicolor filters without the objective prism; b) the spectroscopy pipeline to analyze data taken with the objective prism; and, c) the supernova pipeline, a highly specialized program used in the search for type Ia Supernovae and other variable objects. The output of these pipelines are typically object catalogs which form the starting points of more specialized data analysis programs. Examples of these programs include searching for variable objects such as RR Lyrae stars, TNOs, quasars, etc., or identifying quasars by their colors (in direct data) or broad emission lines (in objective prism data).

5.2. The Photometry Pipeline

This program was developed to analyze data taken in direct mode (without the objective prism) using multicolor filters — typically U, B, U, V, or R, B, R, V. Data from repeated scans of the same area of the sky are co–added. One color, usually V or R, is selected as the lead color and is used to find objects. The locations of the objects found in the lead color are translated to the coordinate system of each of the other colors for each night of data and photometry, using both aperture photometry and PSF (Point Spread Function) fitting, is carried out to obtain magnitudes in each color. Landoldt standards (Landolt 1992) or secondary standard stars are used for photometric calibration. The astrometric calibration is carried out using the USNO A2.0 catalog (Monet et al. 1999); the typical resulting precision is about $0.2''$. A more detailed description of this pipeline will be published in a separate article.

5.3. The Spectroscopy Pipeline

This program has been developed (Sabbey 1999b) to analyze drift scan data taken with the objective prism. Data from repeated scans of the same region of the sky are co–added. From the

co–added data, spectra of individual objects are extracted, background subtracted and calibrated. The program then automatically examines each spectra and selects objects with prominent emission lines from which redshifts can be determined (Sabbey 1999c). A typical objective prism spectrum with two broad emission lines, identified by the program is shown in figure 15.

5.4. The Supernova Pipeline

This program was developed by the Supernova Cosmology Project (**?**, see, for example,)]Perlmutter1999 and was adapted to work with the output of the QUEST Camera in drift scan mode. In this program, data from "discovery" nights and from "reference" nights (typically about two weeks earlier than the discovery nights) are convolved to the same seeing and normalized to the same intensity scale. The reference nights are then subtracted pixel–by–pixel from the discovery nights. The vast majority of the objects disappear in the subtraction. Objects with significant residuals in the subtraction are examined visually as candidates for variable objects such as supernovae, trans–Neptunian objects, asteroids, etc.

6. Performance of the Apparatus

The QUEST camera was commissioned in the Venezuelan Schmidt telescope in 1997. We have had three observing seasons from November 1998 to May of 2001. Using these observations, the performance of the combination of the camera, the telescope, and the site of Llano del Hato have been fairly well characterized.

6.1. Alignment Procedure

During the initial commissioning phase, the plane of the front surfaces of the CCDs had to be aligned to be parallel to the focal plane to within the $\pm 25\,\mu$m depth of field of the telescope. This was done by tilting adjustments around the two relevant rotational degrees of freedom. The method used was to precisely measure the optimal focus position of each individual CCD. The most sensitive method used a Hartmann mask (a sheet at the entrance of the telescope with a pattern of small holes) which produces double images when the CCDs are not in focus. The image separation is proportional to the offset from the best focal position. By taking two exposures, one well below and the second well above focus, the precise focal position of each CCD could be determined. Initially, when the CCD plane was not exactly parallel to the telescope focal plane, a systematic tilt in these focal positions was observed. After several interations of adjusting the tilt angle and repeating the Hartmann mask test, the CCD plane was brought into the telescope focal plane well within the depth of field. A check of the adequacy of this alignment is to examine the full width half maximum (FWHM) of the Point Spread Function (PSF) of the images in the individual CCDs

at a single focal position of the entire camera. Such a set of measurements is shown in figure 9. No systematic variation of the FWHM across the diagonal of the full image plane is observable. This alignment procedure, carried out during commissioning, did not have to be repeated except once after the camera was taken out of the telescope for maintenance.

The rotational position of each of the four fingers and the readout clocking rate synchronization has to be optimized or checked every time the declination of the drift scan is changed. The expected finger position and clocking rates are calculated and set by the control computer for the desired declination. At the beginning of observations of a new value of the declination, these settings are optimized by varying the finger positions and the clocking rates in small steps around the expected values. If the finger position is off, the images are elongated in the North–South direction, and if the clocking rate is off, the images are elongated in the East–West direction. The optimum settings are those that produced the smallest, round images. After some experience with the camera, we learned to trust the computer settings and this optimization procedure was undertaken only when the images did not have the expected point–like shape.

6.2. Seeing Quality

During commissioning, the seeing FWHM was in the vicinity of $3''$. A considerable effort was made to improve the ventilation of the dome, putting thermal enclosures vented to the outside around the electronics box and the refrigeratation unit located on the floor near the telescope, and putting servo controlled heaters on the camera body inside the telescope. After these improvements, the seeing was closer to $2''$. In the drift scan mode with effective 140 second exposure times, the best seeing observed was $1.8''$. The distribution of the FWHM during the month of March (1999 and 2000 combined) is shown in figure 16. The median seeing was around $2.4''$. The best seeing in the non-drift scan point and stare mode, with 5 second exposures, is shown in figure 9. The best seeing for these short exposures was $1.5''$. The degradation from $\sim 1.5''$ to $\sim 1.8''$ is consistent with what we expect from the effects of drift scanning discussed in § 2 above.

6.3. Readout noise and sky background

The rms fluctuations (noise) on the output amplitudes of the CCDs have contributions from the read noise inherent in the CCDs, the dark current in the CCDs, the noise introduced by the electronics, pick up noise in the cabling and cross talk, fluctuations in the sky background, and finally the statistical fluctuations of the star light signal itself. The combination of the read noise and dark current in the CCDs, the electronics noise and the pickup noise, was measured by looking at the rms spread of the signals of dark exposures. This combined noise varied from 9 to 21 electrons with a median of 13 electrons per pixel.

The sky background depends strongly on the color filters used. For a dark night, it is smallest,

around 20 electrons/pixel/140 seconds with the U filter, and largest, around 600 electrons/pixel/140 seconds with the R filter. Typical values of the sky background with the different filters used are given in table 5. These backgrounds, of course, also vary a fair amount with the phase of the moon and the atmospheric conditions. Under normal conditions we are read noise limited in the U and B filters, but sky noise limited in the V and R filters.

6.4. Limiting Magnitudes and Photometric Errors

We take the limiting magnitudes to be the magnitude of objects for which the signal to noise is larger than 10 to 1, or the total error on the magnitude of the object is less than 0.1 magnitudes. The limiting magnitudes depend strongly on the color filter used, and also on the phase of the moon and the atmospheric conditions. We estimate the limiting magnitude by plotting the error in the measured magnitude versus the magnitude with a given filter. An example of such a plot is shown in figure 17. This plot is for a single CCD with 140 second drift scan exposures over a number of nights with dark moon, so the spread in the points is primarily due to atmospheric conditions. The curve crosses the 0.1 mag error line between magnitudes 18.8 and 19.4 which we take to be the limiting magnitude. The typical limiting magnitudes are given in table 5. At the bright end, stars saturate the CCDs around magnitude 13.

The assigned photometric errors on the measured magnitudes were calculated in the photometric pipeline program. The correctness of these assigned errors was checked by looking at repeated measurements of the same objects observed in about 20 repeated scans of the same area of the sky in March of 1999 and 2000. The photometric program corrected for variations in atmospheric extinction from night to night. After these corrections, the rms spread of the actual individual measurement of the same object agreed well with the error calculated by the program. For bright objects, around magnitude 15 or 16, the errors were as low as 0.002 magnitudes. The errors discussed above do not include the photometric calibration errors; these depend on the number and proximity of the standard stars used in the calibration.

6.5. Scientific Results

During the first three years of operation of the CCD camera we obtained a survey of 700 square degrees with the objective prism, a survey of 1000 square degrees with color filters and a 250 square degree variability survey with repeat time scales varying from twice a night to three years. Some of the scientific results obtained include a quasar correlation and large scale structure study (Sabbey et al. 2001), discovery of the optical counterpart of a gamma ray burster (Schaefer et al. 1999), discovery of a new minor planet 2000 EB173 (Ferrin et al. 2001), an RR Lyrae survey (Vivas et al. 2001), a star formation and T Tauri star study (Briceño et al. 2001), a sample of about 30 type Ia supernovae (Snyder et al. 2002), and a sample of about 5000 quasars indentified by a variety of

techniques (Andrews et al. 2002).

As an example of the quality of the data, figure 18 shows a UBV color–color diagram of a typical observation. There is a narrow concentration where we expect the main sequence stars, the overall random background is small, and there is a small concentration in the region where we expect quasars with redshifts below 2.2. Spectroscopic followup has demonstrated that the efficiency of this quasar sample is around 65% and comparison with catalogs of known quasars indicate a completeness around 70%.

REFERENCES

Andrews, P. A. et al. 2002, in preparation

Bessel, M. S. 1990, PASP, 102, 1181

Briceño, A. et al. 2001, Science, 291, 93

Ferrin, I. et al. 2001, Astrophys. J., 548, L243

Landolt, A. U. 1992, Astron. J., 104, 340

Loral–Fairchild Imaging, Inc. 2001, CCD 442A Datasheet, http://www.fairchildimaging.com/main/documents/ccd442a.pdf

McGraw, J. T., Cawson, M. G. M., & Keane, M. J. 1986, in Instrumentation in astronomy VI; Proceedings of the Meeting, Tucson, AZ, Mar. 4-8, 1986. Part 1 (A87-36376 15-35). Bellingham, WA, Society of Photo-Optical Instrumentation Engineers, 1986, p. 60-69., Vol. 627, 60–69

Monet, D. et al. 1999, USNO–A2.0 (U.S. Naval Observatory, Washington DC)

Perlmutter, S. & The Supernova Cosmology Project. 1999, Astrophys. J., 517, 565

Pravdo, S. 2002, NEAT/Palomar Instrument Description, http://neat.jpl.nasa.gov/neatoschincam.htm

Sabbey, C. N. 1999a, in ASP Conf. Ser. 172: Astronomical Data Analysis Software and Systems VIII, 129

Sabbey, C. N. 1999b, in ASP Conf. Ser. 172: Astronomical Data Analysis Software and Systems VIII, 207

Sabbey, C. N. 1999c, PhD thesis, Yale University

Sabbey, C. N., Coppi, P., & Oemler, A. 1998, PASP, 110, 1067

Sabbey, C. N. et al. 2001, Astrophys. J., 548, 585

Schaefer, B. E., Snyder, J. A., et al. 1999, Astrophys. J., 524, L103

Snyder, J. A. et al. 2002, in preparation

Vivas, A. K. et al. 2001, Astrophys. J., 554, L33

AAS LaTeX macros v5.0.

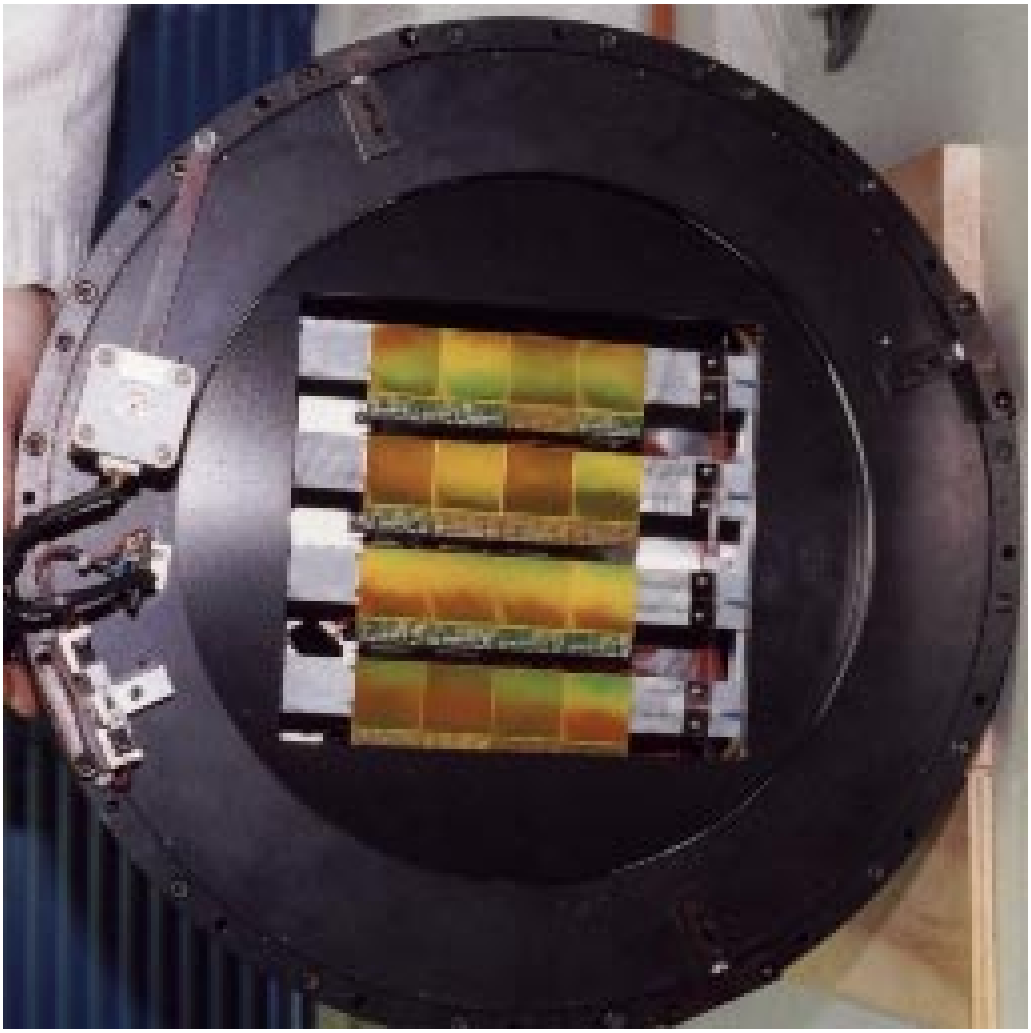

Fig. 1.— A picture of the QUEST camera. The drift direction is from the top towards the bottom.

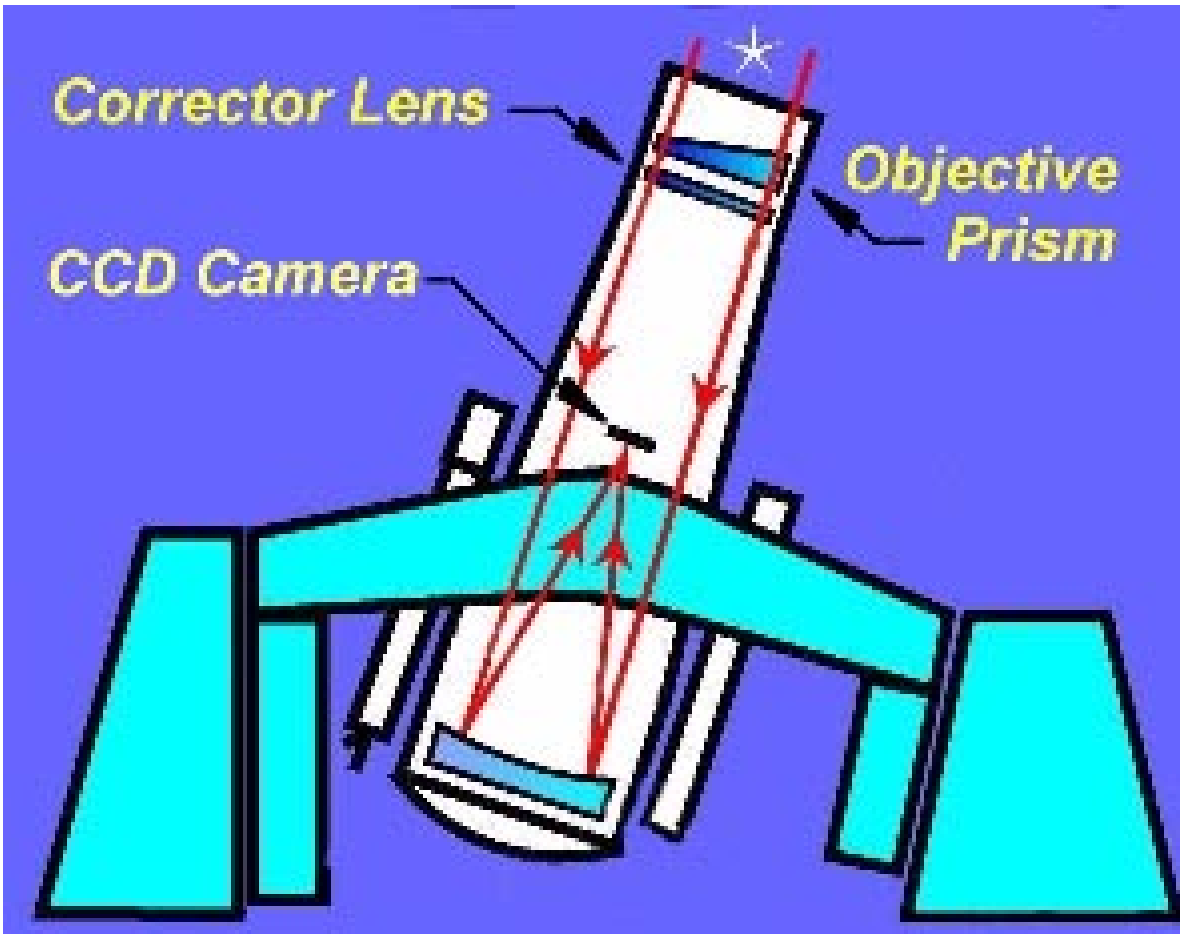

Fig. 2.— The Venezuelan Schmidt telescope showing the QUEST camera at the prime focus. Note that the prism angle is exaggerated and the bending of the input rays is neglected.

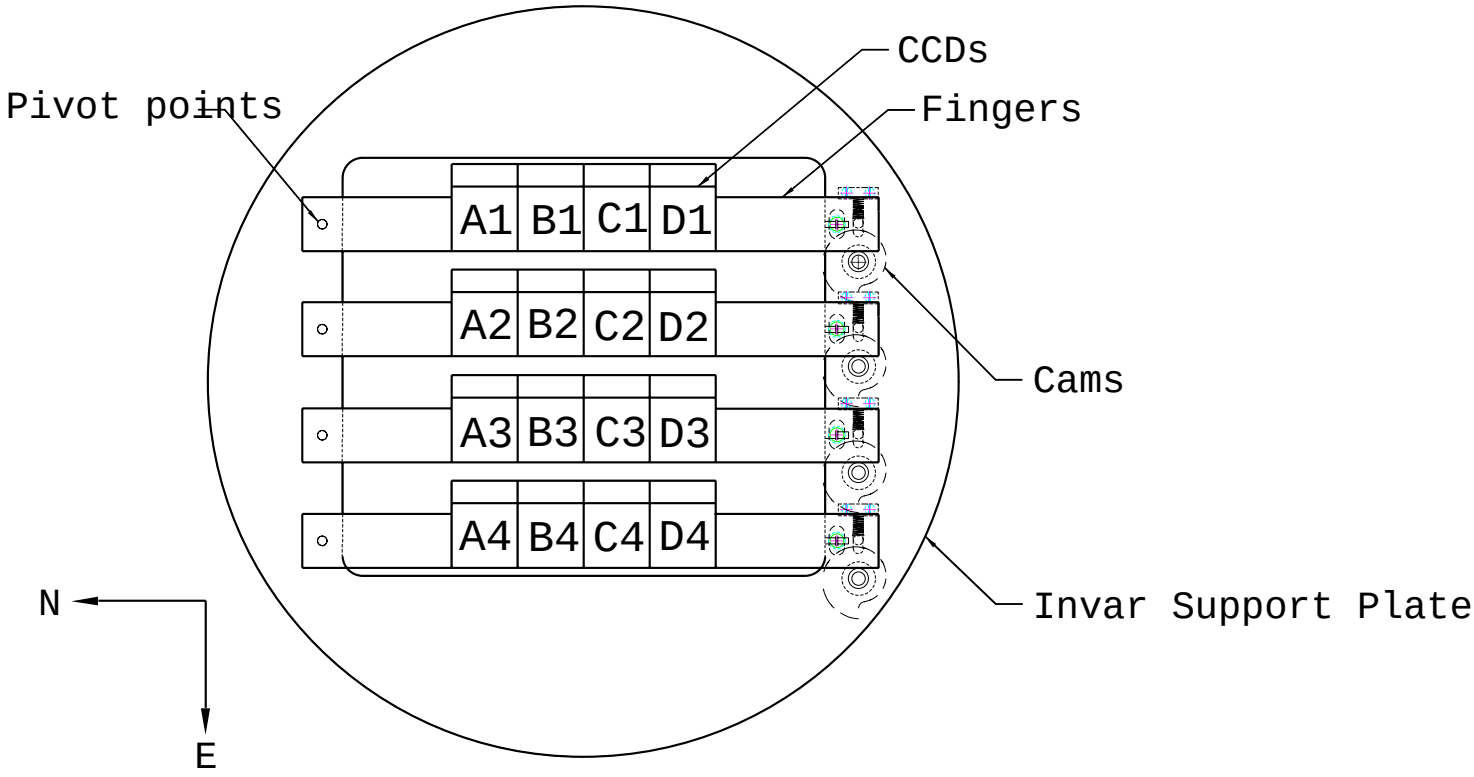

Fig. 3.— Layout of the CCDs on the image plane. Also shown are the Invar fingers supporting the CCDs, their pivot points and the finger rotating cams.

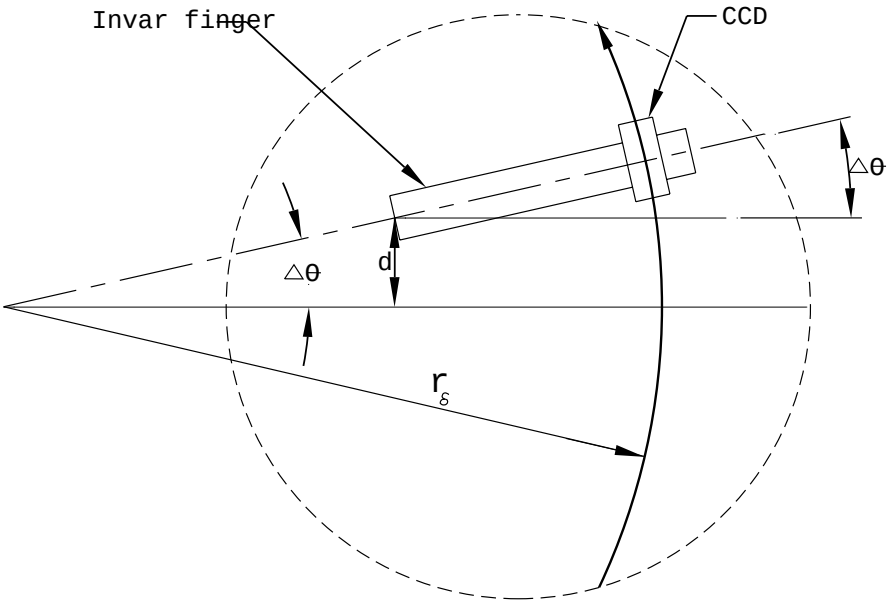

Fig. 4.— Schematic diagram of the CCD rotation to keep each CCD lined up along the line of motion of the star images.

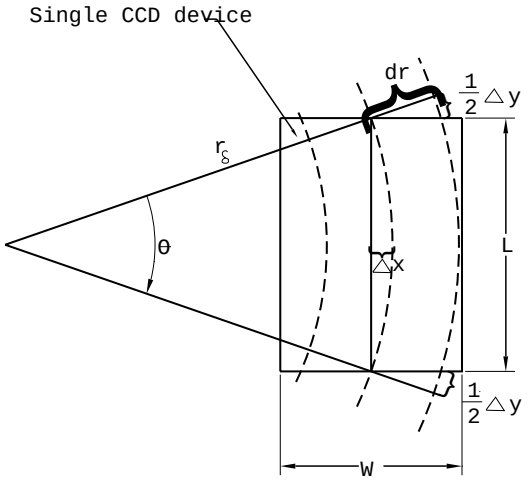

Fig. 5.— Sagitta (Δx) and path length difference (Δy) on a single CCD.

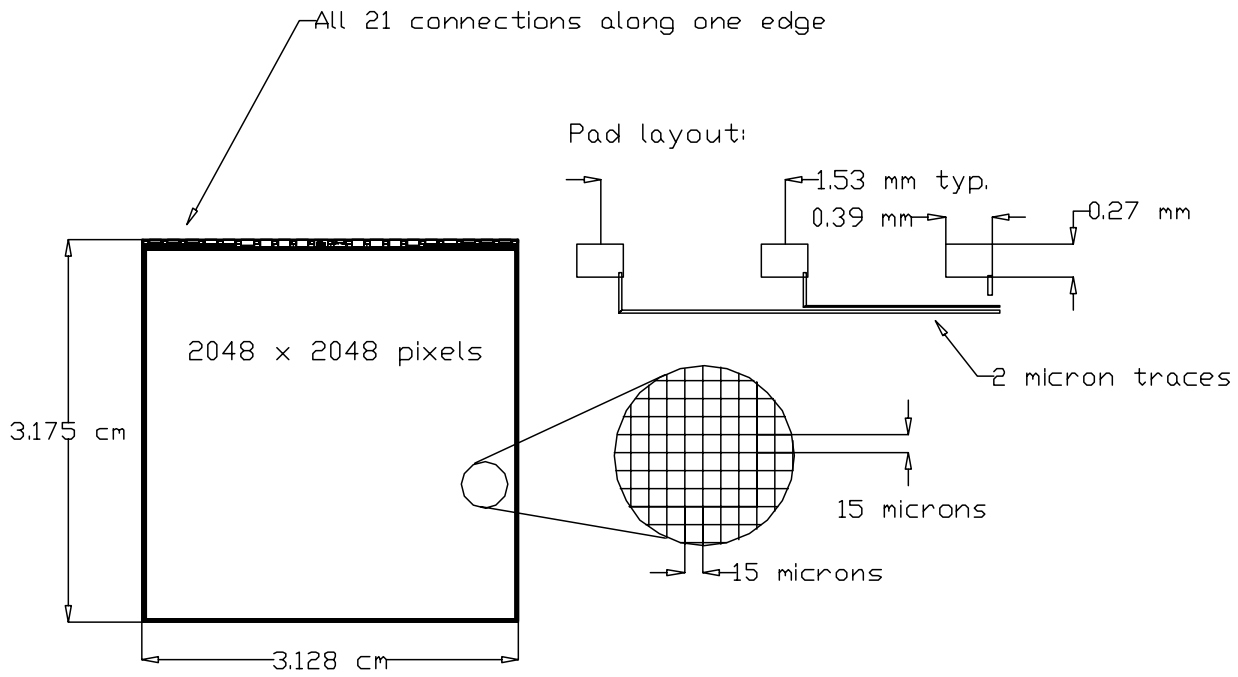

Fig. 6.— Sketch of the CCDs with 2048 × 2048 15 μm × 15 μm pixels.

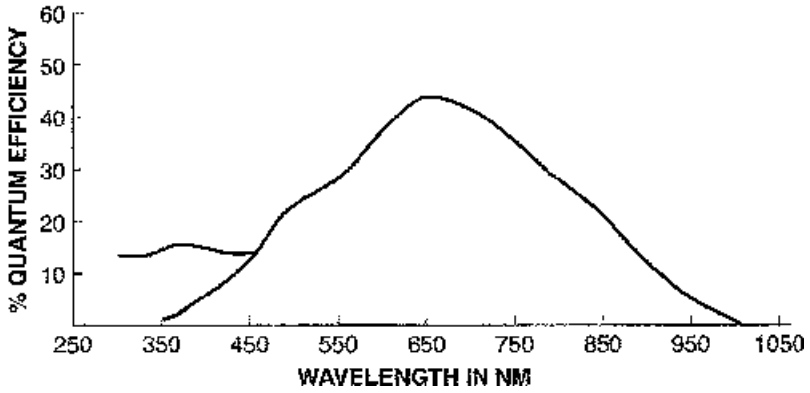

Fig. 7.— Typical quantum efficiency of front illuminated commercial Loral CCDs. The response below 4000 Å is due to a wavelength shifting compound on the front surface.

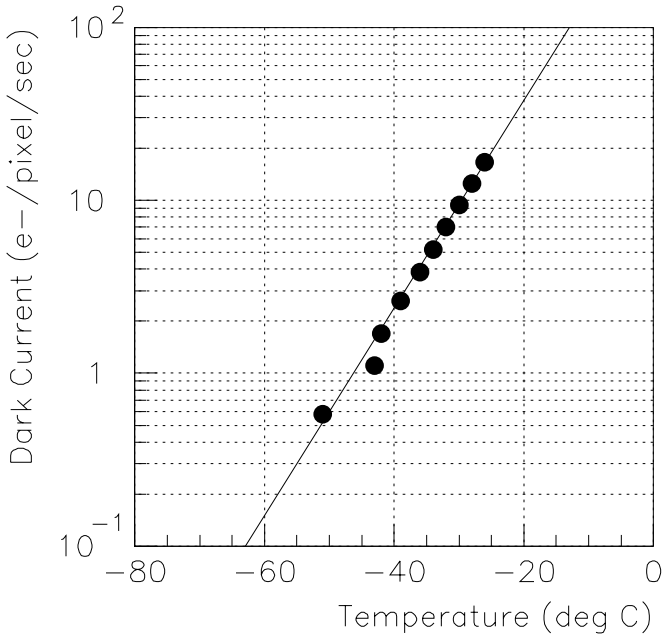

Fig. 8.— Typical dark current versus temperature plot for the CCDs.

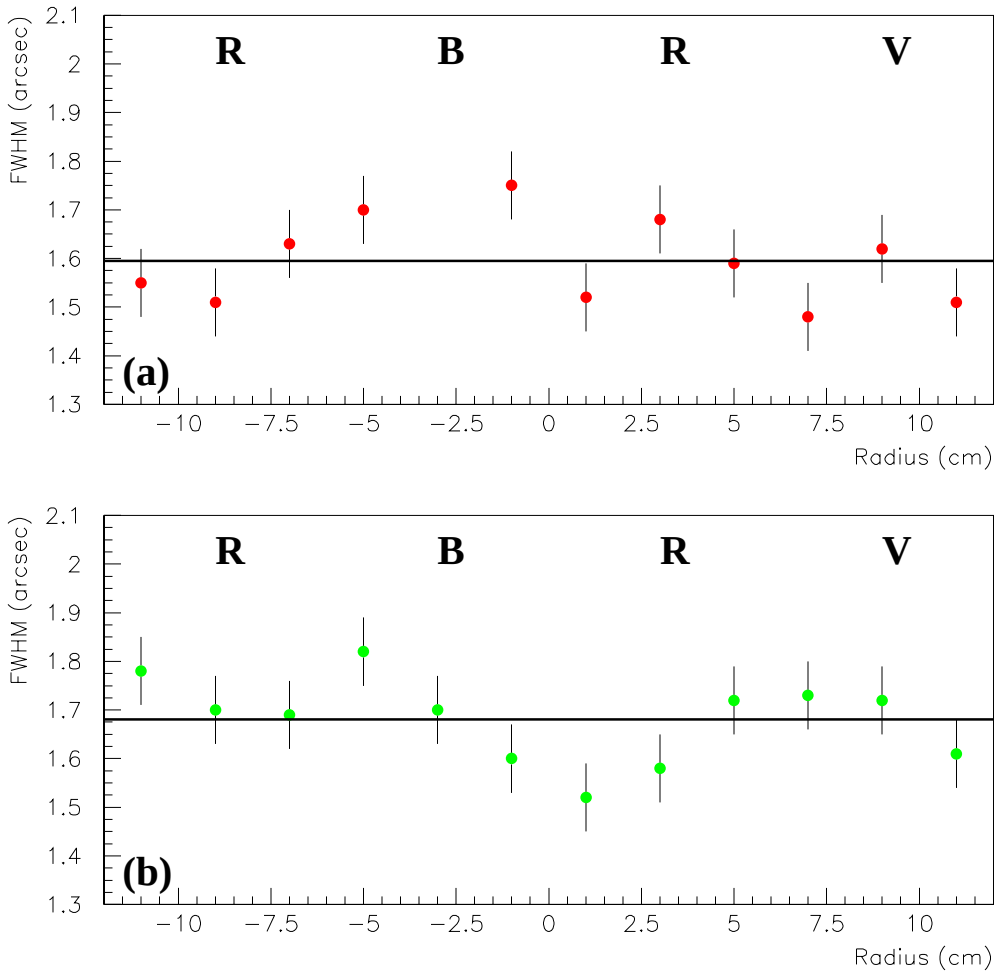

Fig. 9.— The average stellar full width at half maximum (FWHM) along the two diagonals of the full image plane for a typical exposure: (a) across CCDs A1, B2, C3 and D4 and (b) across CCDs A4, B3, C2 and D1. The fifth point in (a) is omitted since there were insufficient stars in the data.

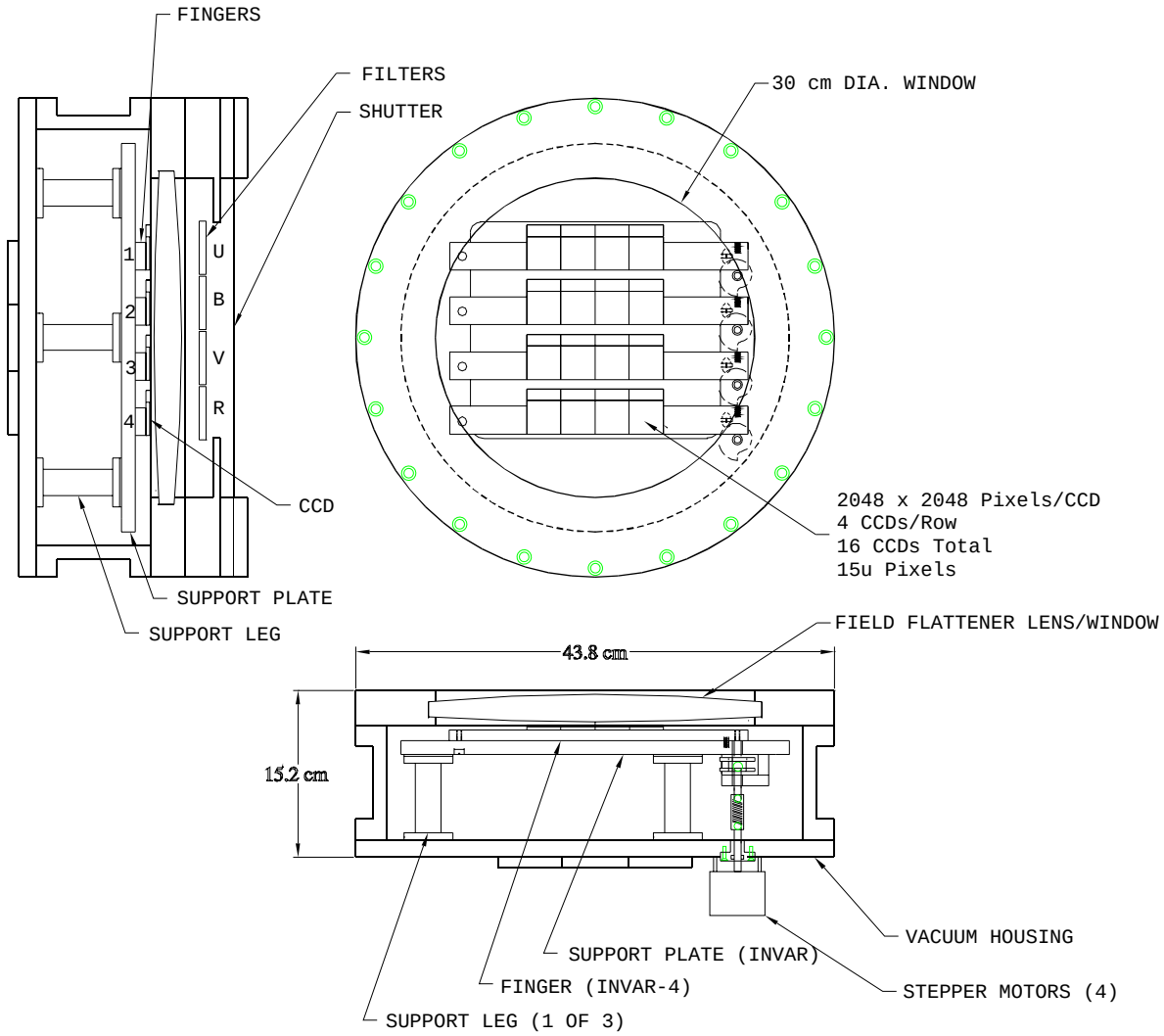

Fig. 10.— Frontal view and two cross–sectional views of the QUEST camera.

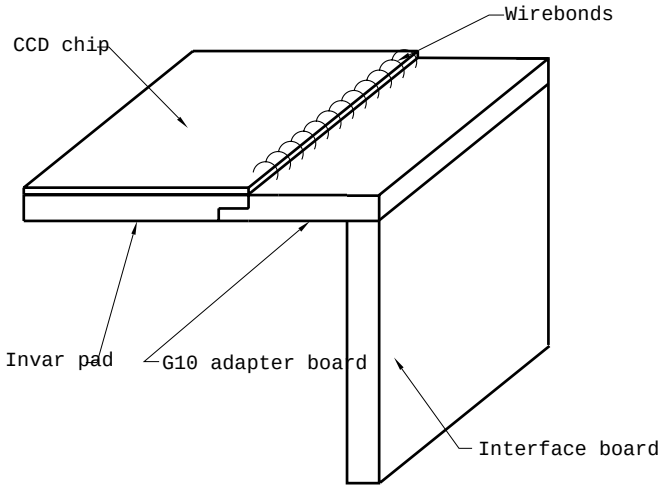

Fig. 11.— The CCD packages.

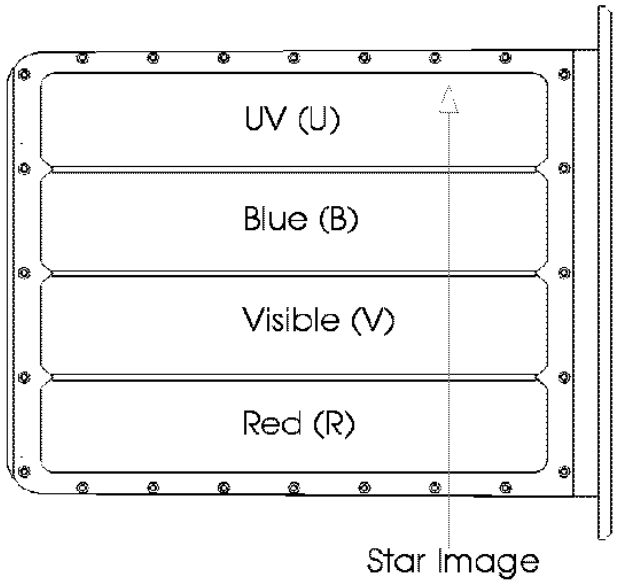

Fig. 12.— The filter tray with four typical color filters.

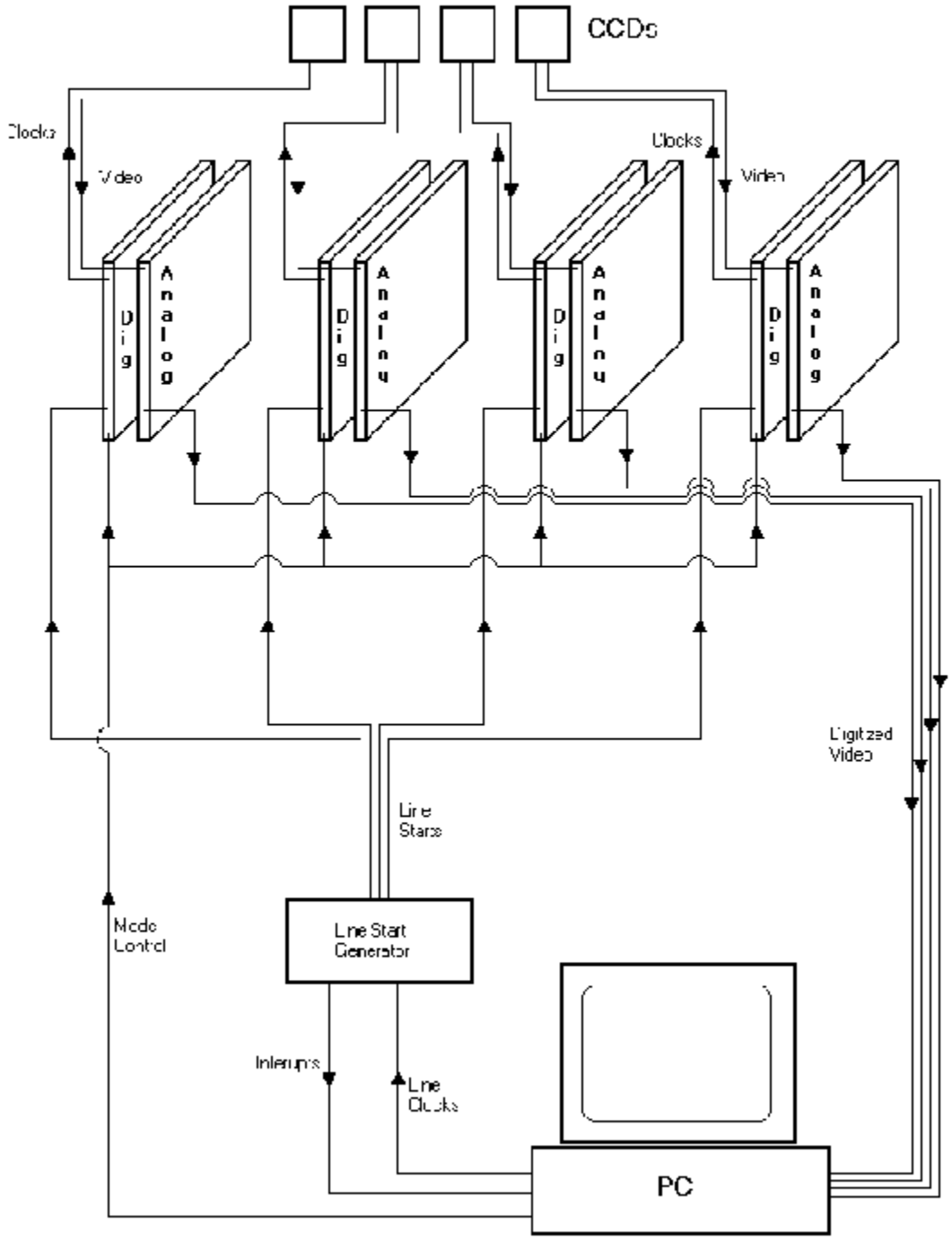

Fig. 13.— Schematic of the CCD detector read–out and control system.

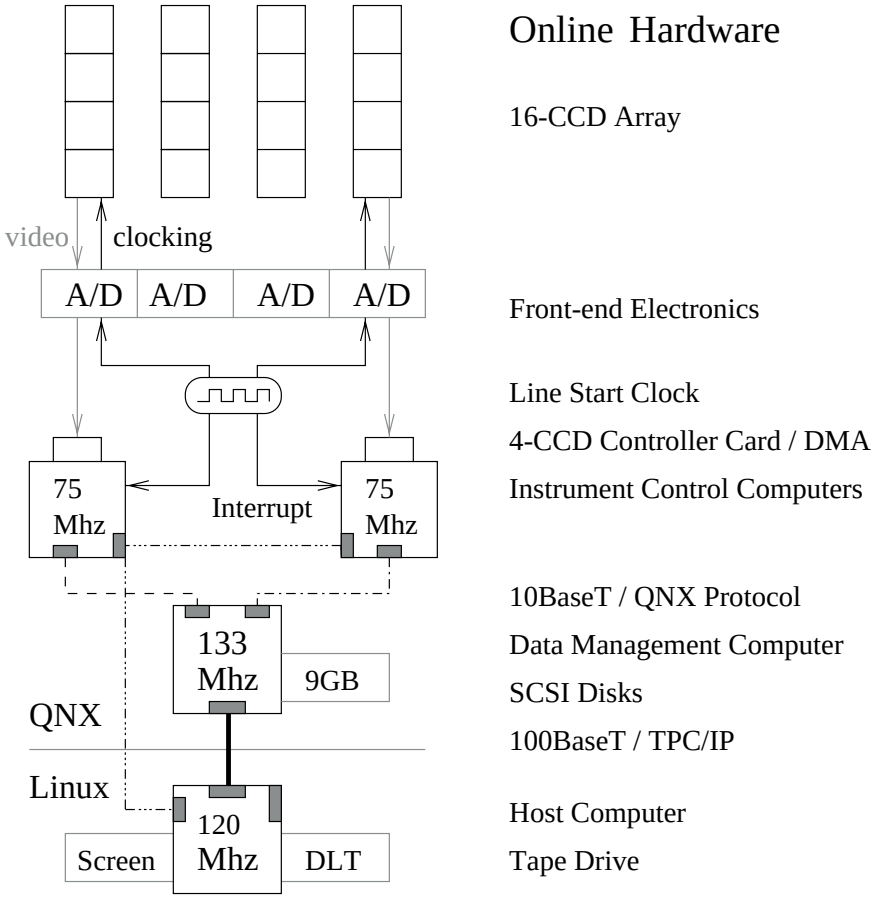

Fig. 14.— Block diagram of the data acquisition system.

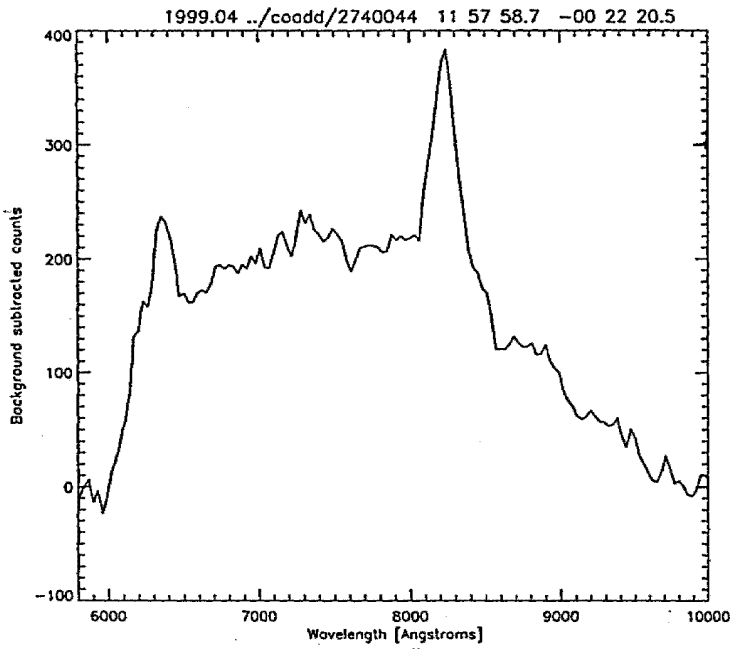

Fig. 15.— The objective prism spectrum of a $z = 0.25$ QSO with two broad emission lines identified by the spectroscopy analysis program.

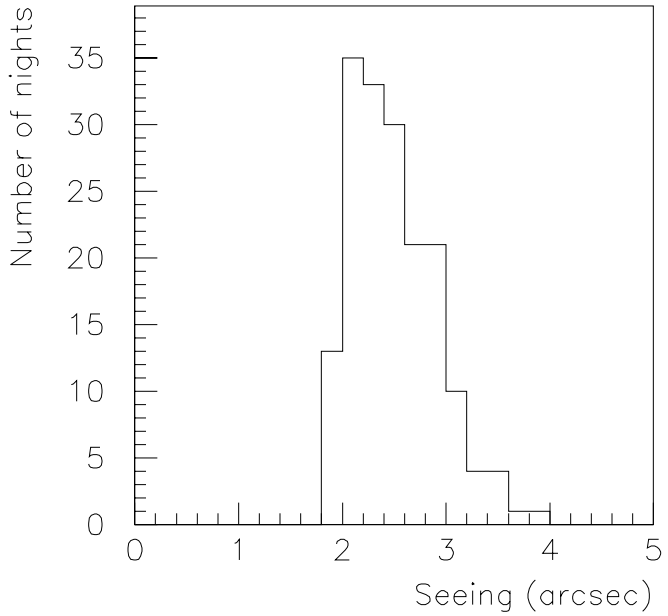

Fig. 16.— Distribution of the image FWHM of data taken in March 1999 and 2000.

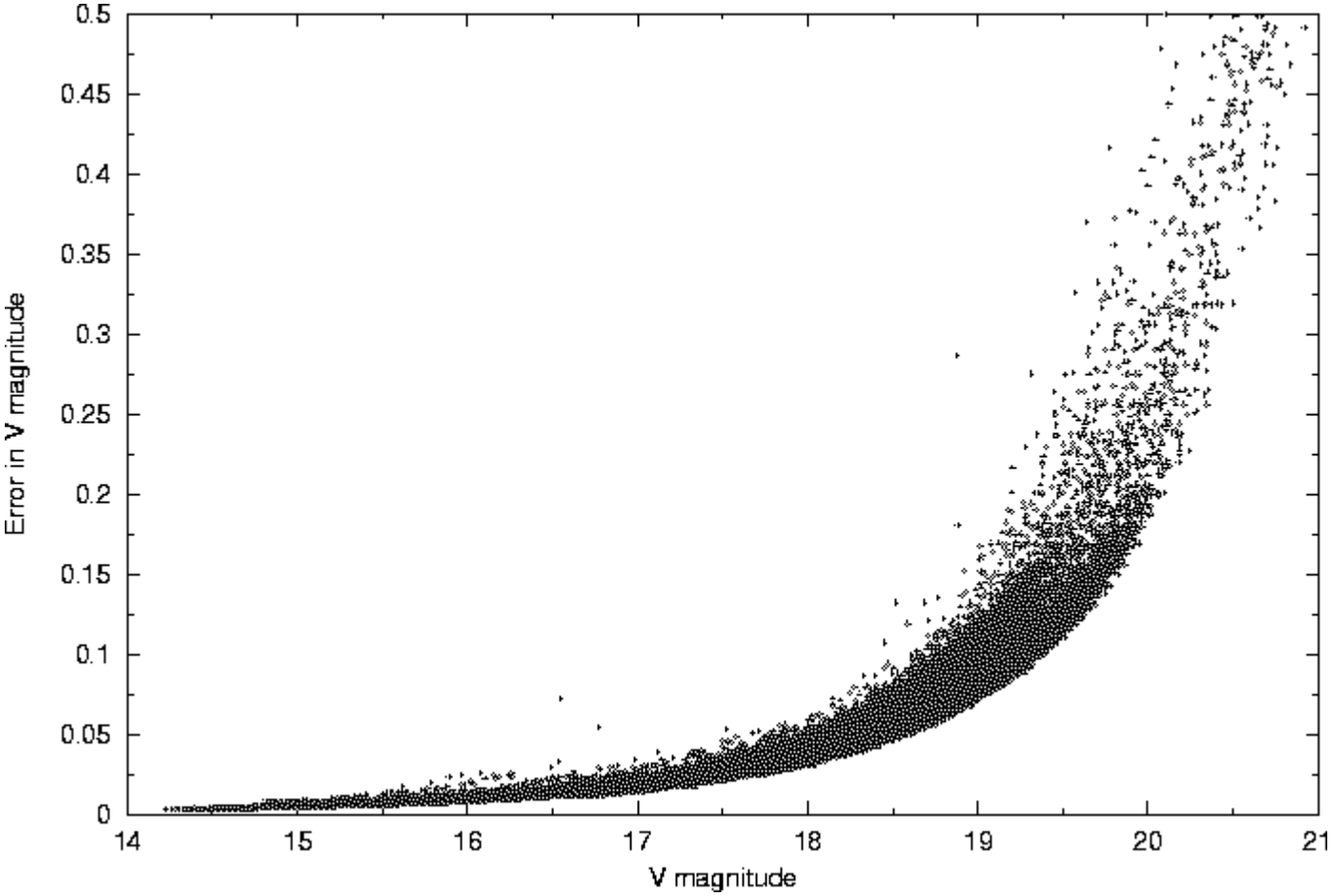

Fig. 17.— Plot of the error on the magnitude versus the magnitude with the V color filter.

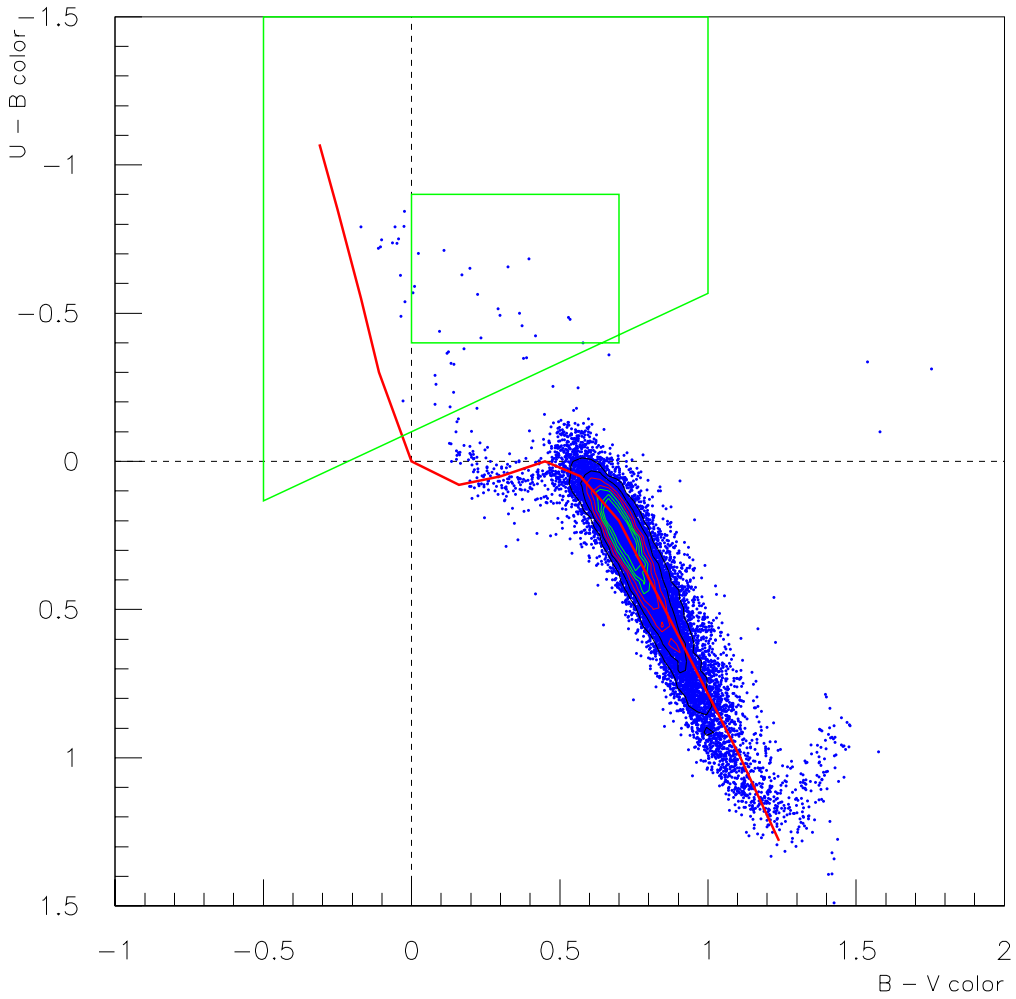

Fig. 18.— The UBV color–color diagram, showing clustering along the main sequence line and quasar candidates in the expected region.

Parameter	Value
Clear aperture diameter	1.00 m
Mirror diameter	1.52 m
Focal length	3.03 m
f ratio	$f/3$
Plate scale	15 μm/arcsec (67 arcsec/mm)
Corrector plate glass	UBK7
Objective prism:	
Aperture Diameter	1.0 m
Wedge angle	3.3°
Dispersion	650 Å/ mm at 4350 Å
Glass	UBK7
Latitude of observatory	8° 47′ North
Longitude of observatory	-70° 52′ 0″
Elevation	3600 m

Table 1: Properties of the Venezuelan Schmidt Telescope

Parameter	Value
Number of CCDs	16
Array size, CCDs	4×4
For each CCD:	
pixel size	15 μm $\times$ 15 μm
Number of pixels	2048×2048
Pixel size on sky	$1'' \times 1''$
Array size, pixels	8192×8192 pixels
Array size, cm	12.6 cm $\times$ 18.2 cm
Array size, on sky	$2.3° \times 3.5°$
Effective area	5.4 square degrees

Table 2: Properties of the QUEST camera

Parameter	Value
CCD size, mm	31.28mm × 31.75 mm
CCD size, pixels	2048 × 2048
Pixel size	15 μm × 15 μm
CCD type	Front illuminated
Clocking rate in drift scan mode:	
parallel clock	$\sim$ 15 rows/sec
serial clock	50 kilohertz
Read noise	$\sim$ 10 electrons
Dark current at 20°C	250 pA/cm^2
Full well capacity	30,000 to 60,000 electrons
Quantum efficiency:	
at 7000 Å	$\sim$ 45%
below 4000 Å	5 to 10%

Table 3: Characteristics of the CCDs used in the camera

Color	Wavelength Range (Å)
U	3300 — 4000
B	3900 — 4900
V	5050 — 5950
R	5900 — 8100
I	7800 — 10,200
Hα	6520 — 6600
Broad B	4000 — 6500
Broad R	6500 — 9000

Table 4: Color filters available for the QUEST camera.

Filter	Typical Sky Background Electrons/pixel/140 seconds	Limiting Magnitude S/N $\geq$ 10
U	20	16.5
B	200	18.5
V	300	19.2
R	600	19.5

Table 5: Typical sky backgrounds for a dark night and limiting magnitudes for a single 140 second exposure.

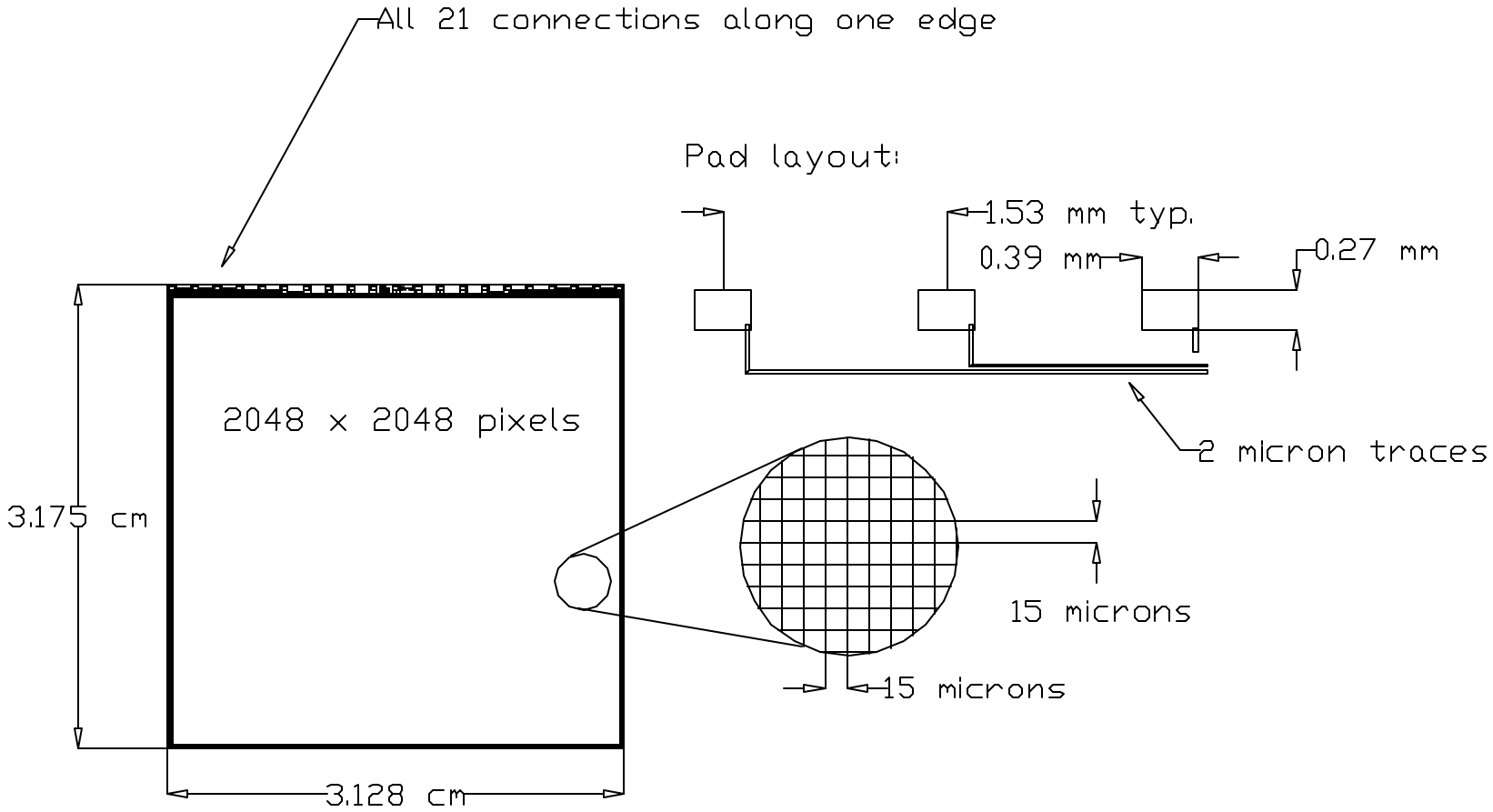
All 21 connections along one edge
Pad layout:
1.53 mm typ.
0.39 mm
0.27 mm
2 micron traces
2048 x 2048 pixels
3.175 cm
3.128 cm
15 microns
15 microns

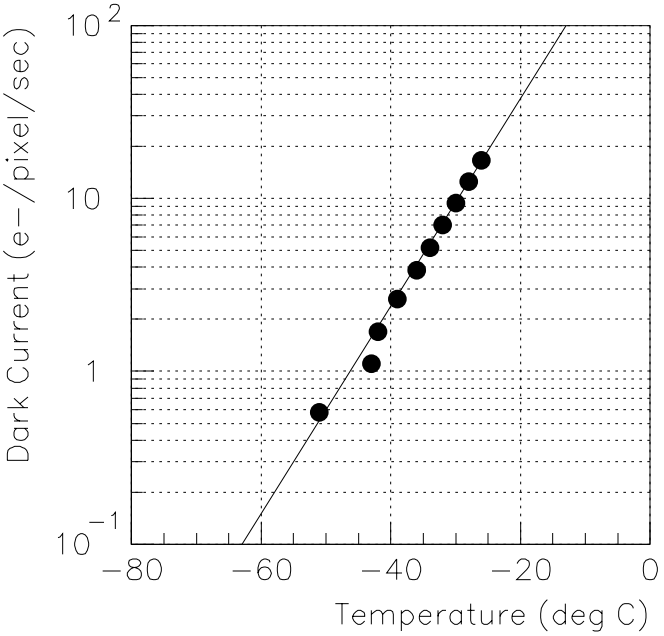
Dark Current (e−/pixel/sec)
10 2
10
1
10 −1
−80
−60
−40
−20
0
Temperature (deg C)

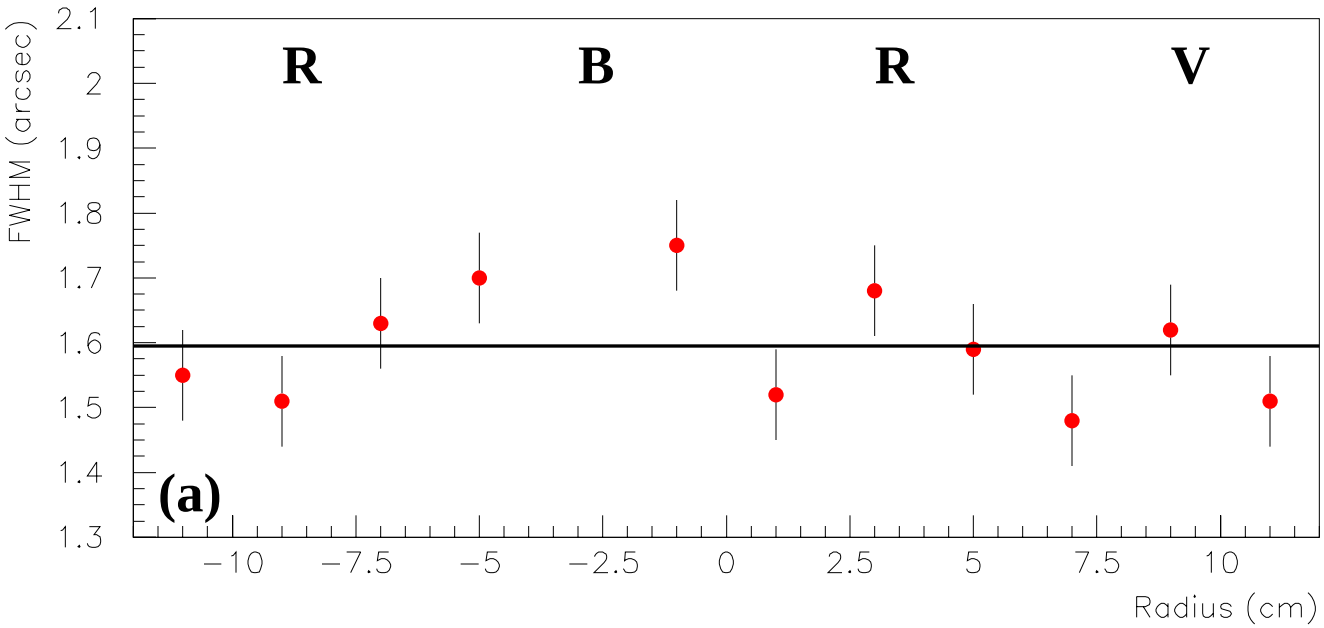
R
B
R
V
(a)
FWHM (arcsec)
2.1
2
1.9
1.8
1.7
1.6
1.5
1.4
1.3
−10
−7.5
−5
−2.5
0
2.5
5
7.5
10
Radius (cm)

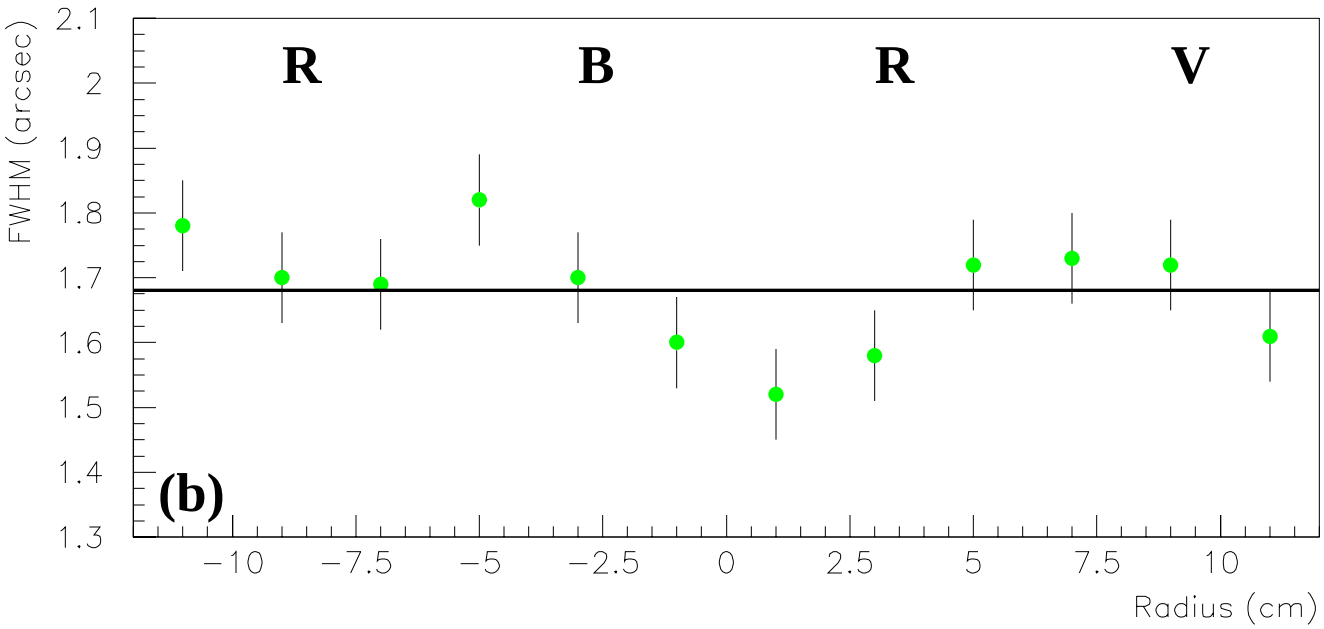
R
B
R
V
(b)
FWHM (arcsec)
2.1
2
1.9
1.8
1.7
1.6
1.5
1.4
1.3
−10
−7.5
−5
−2.5
0
2.5
5
7.5
10
Radius (cm)

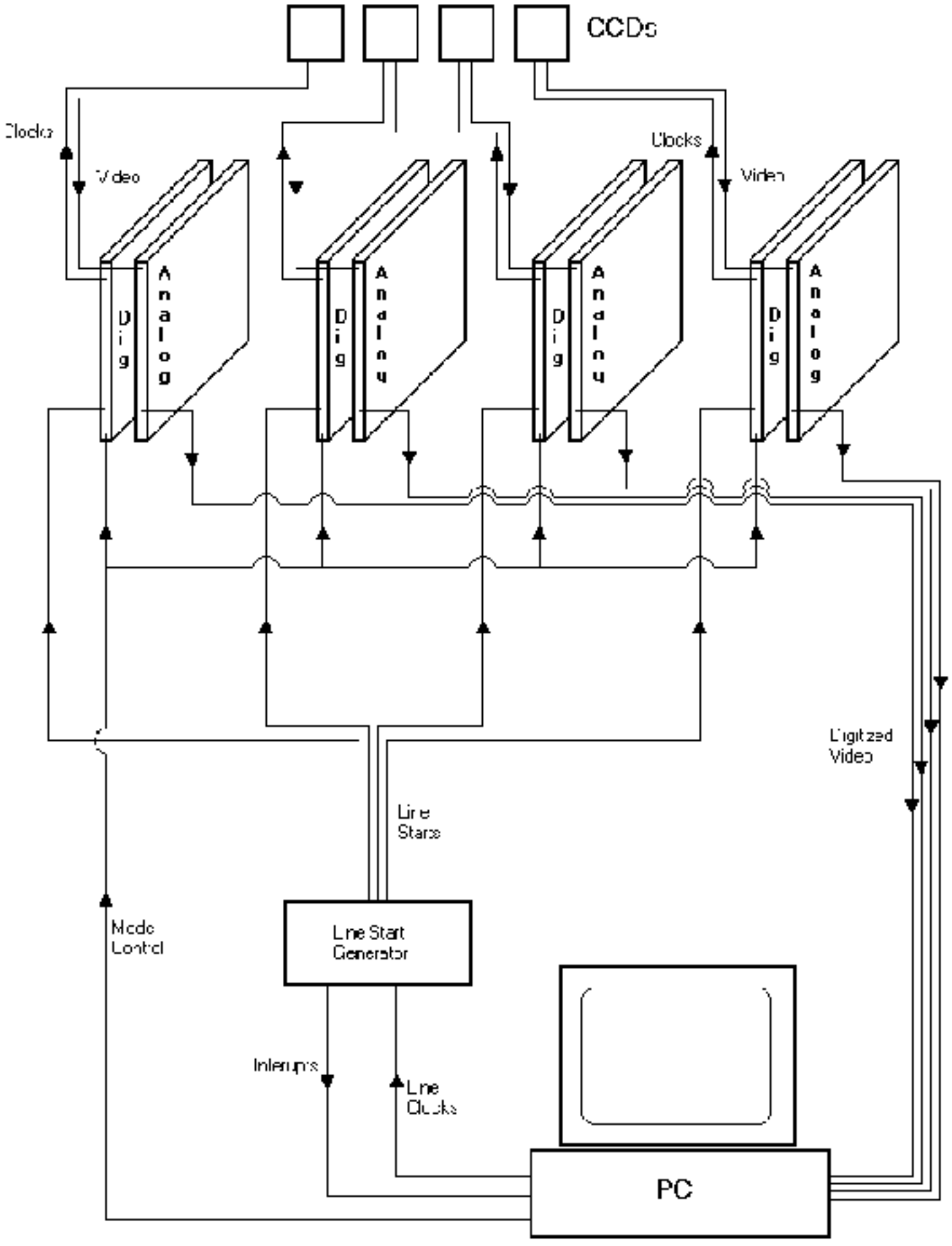
CCDs
Clocks
Video
Clocks
Video
Dig
Analog
Dig
Analog
Dig
Analog
Dig
Analog
Digitized
Video
Line
Start
Mode
Control
Line Start
Generator
Interrupts
Line
Clocks
PC

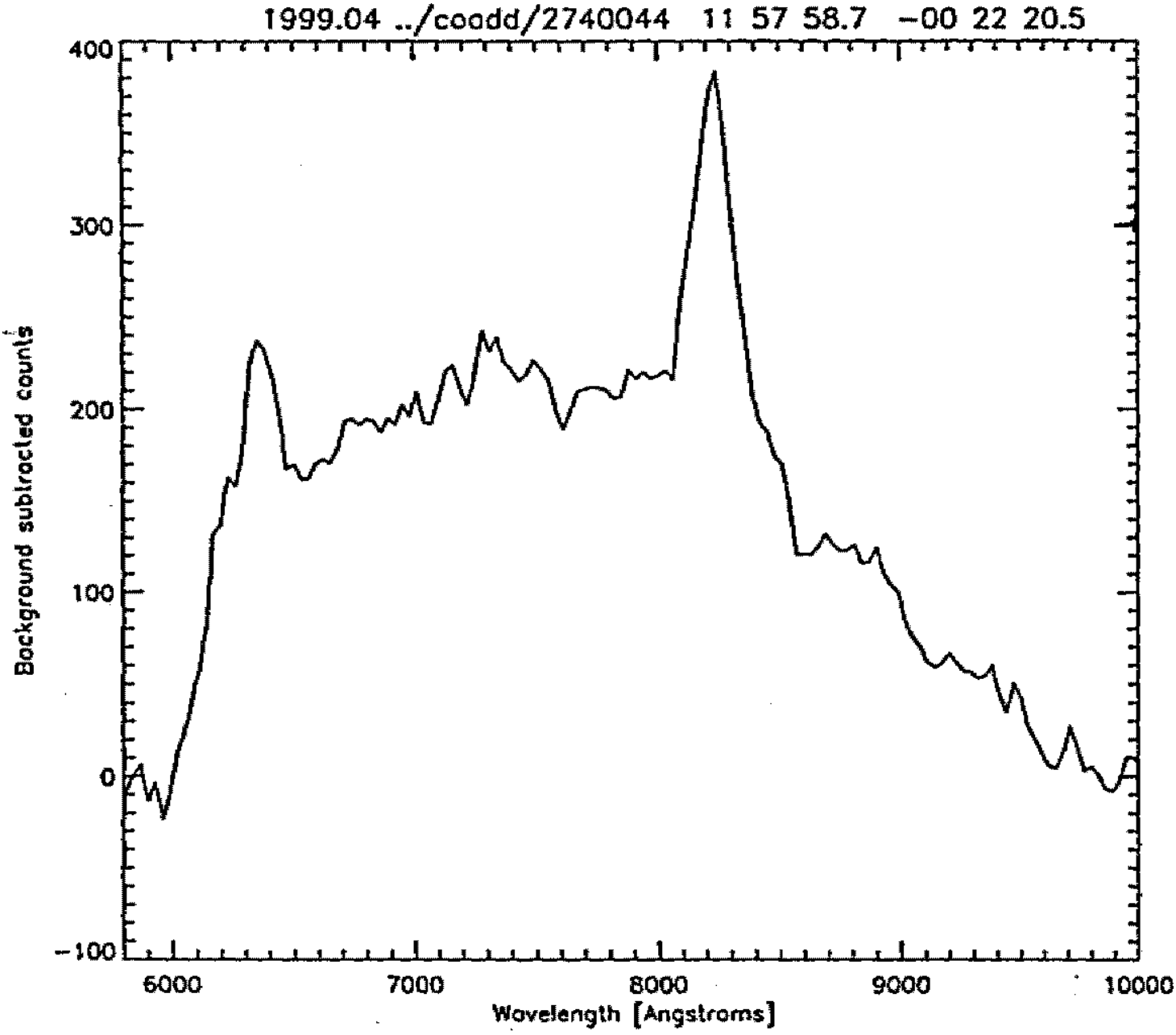
1999.04 ../coodd/2740044 11 57 58.7 -00 22 20.5
400
300
200
100
0
-100
Background subtracted counts
6000
7000
8000
9000
10000
Wavelength [Angstroms]

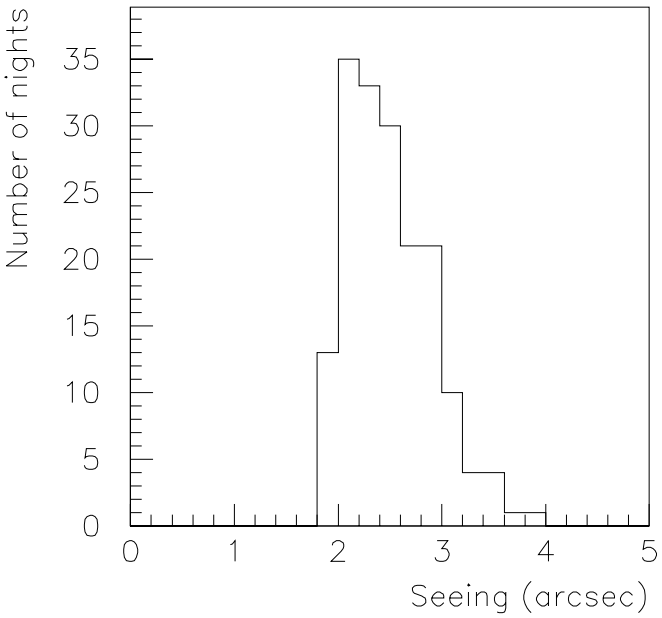
Number of nights
0
5
10
15
20
25
30
35
0
1
2
3
4
5
Seeing (arcsec)

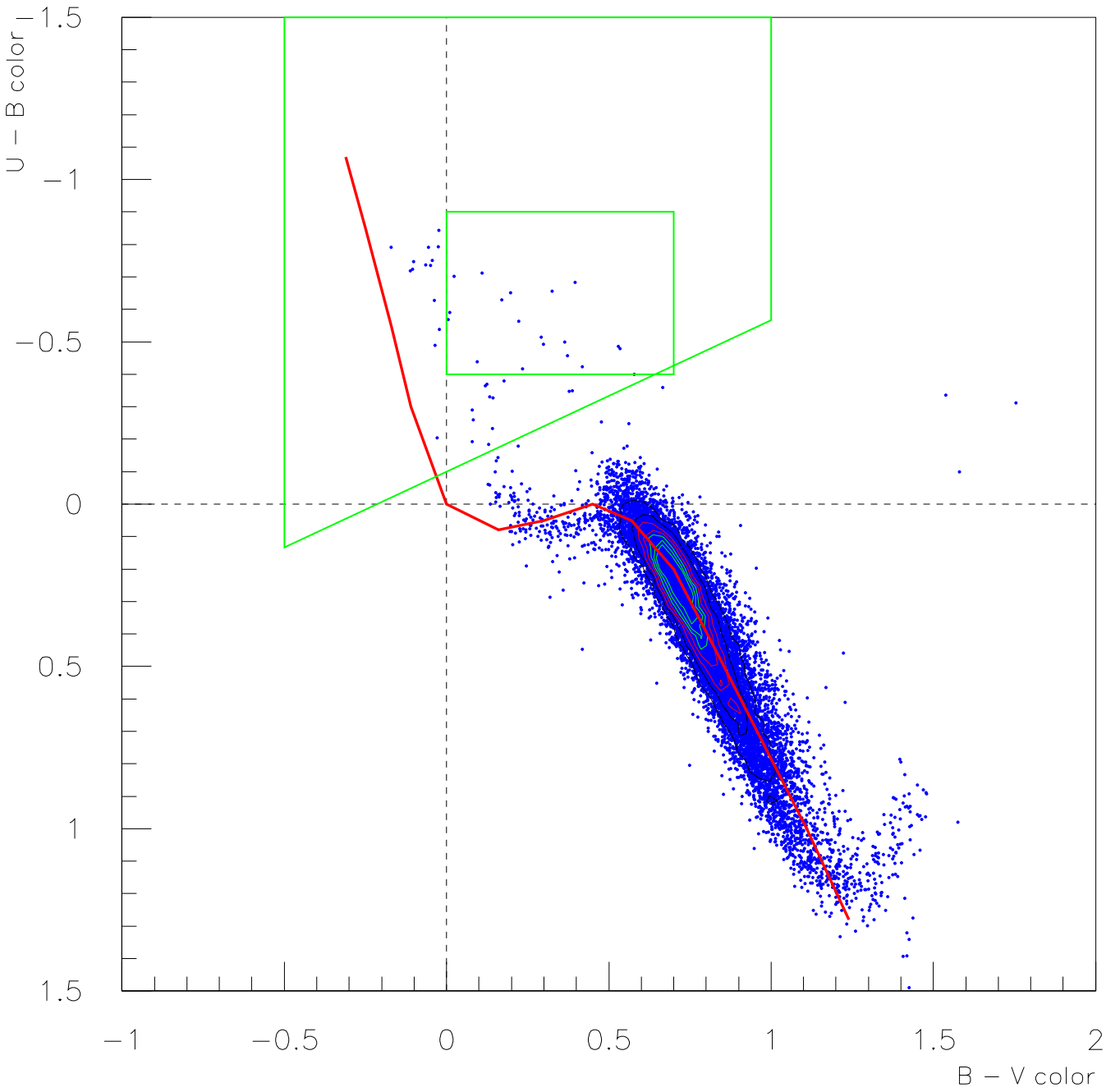
U − B color
1.5
1
0.5
0
0.5
1
1.5
−1
−0.5
0
0.5
1
1.5
2
B − V color